CHARACTERIZATION OF CONDUCTIVE PROPERTIES OF THIN FILMS IN TERAHERTZ REGION

A THESIS SUBMITTED TO
THE GRADUATE SCHOOL OF NATURAL AND APPLIED SCIENCES
OF
MIDDLE EAST TECHNICAL UNIVERSITY

BY

MERVE AKKAYA

IN PARTIAL FULFILLMENT OF THE REQUIREMENTS
FOR
THE DEGREE OF MASTER OF SCIENCE
IN
THE DEPARTMENT OF PHYSICS

AUGUST 2017

Approval of the thesis:

CHARACTERIZATION OF CONDUCTIVE PROPERTIES OF THIN FILMS IN TERAHERTZ REGION

Submitted by **MERVE AKKAYA** in partial fulfillment of the requirements for the degree of **Master of Science in Physics Department, Middle East Technical University** by,

Prof. Dr. Gülbin Dural Ünver
Dean, Graduate School of **Natural and Applied Sciences**

Prof. Dr. Altuğ Özpineci
Head of Department, **Physics**

Prof. Dr. Hakan Altan
Supervisor, **Physics Dept., METU**

Assoc. Prof. Dr. Cumali Sabah
Co-supervisor, **Electrical and Electronics Engineering Dept., METU-NCC**

Examining Committee Members:

Assoc. Prof. Dr. Asaf Behzat Şahin
Electrical and Electronics Engineering Dept., YBU

Prof. Dr. Hakan Altan
Physics Dept., METU

Assoc. Prof. Dr. Serhat Çakır
Physics Dept., METU

Assoc. Prof. Dr. Alpan Bek
Physics Dept., METU

Assoc. Prof. Dr. Okan Esentürk
Chemistry Dept., METU

Date: August 9, 2017

I hereby declare that all information in this document has been obtained and presented in accordance with academic rules and ethical conduct. I also declare that, as required by these rules and conduct, I have fully cited and referenced all material and results that are not original to this work.

Name, Last name :

Signature :

ABSTRACT

CHARACTERIZATION OF CONDUCTIVE PROPERTIES OF THIN FILMS IN TERAHARTZ REGION

Akkaya, Merve
M.S., Department of Physics
Supervisor : Prof. Dr. Hakan Altan
Co-Supervisor : Assoc. Prof. Dr. Cumali Sabah

August 2017, 63 pages

Electrical and optical characterization of thin films has been studied for almost the past thirty years in the terahertz region. In the last few years promising thin film candidates such as vanadium dioxide (VO_2) and various superconductors have opened up a new era of possibilities in terahertz optical electronics. Vanadium dioxide's and superconductors conductivity is of particular interest since vanadium dioxide's conductivity changes when temperature is above the critical temperature and also conductivity of superconductors at room temperature differ from those at low temperature. In this study, the conductivity of thin films made of vanadium dioxide, superconductors on dielectric (sapphire, fused silica) substrates was investigated using experimental methods based on in-house developed spectroscopy systems aided by analytical and numerical simulations of the layered media. Furthermore, such conductivity tunable materials can be especially important for developing devices that work in the terahertz region which historically has been a challenge. Metamaterials and two dimensional type of metamaterials called metasurfaces have an important role to fill this so called THz Gap. After analyzing the conductive properties of films based on yttrium barium copper oxide (YBCO),

gold and VO_2 in the THz region various metasurface designs were simulated for THz transmission using commercially available software, Computer Simulation Technology (CST), Microwave Studio. The simulations were carried out at the various temperatures where the materials showed unique conductive properties and compared to measurements done for single layer YBCO, quadcross shape patterned gold and YBCO film, as well as unpatterned VO_2 at different temperatures by using terahertz (THz) time domain spectroscopy (TDS) system. A closed cycle cryostat is used for controlling the temperature. Therefore, it is found that critical temperature of YBCO film is nearly at 90K and below the critical temperature YBCO film behaves as metal. When temperature is decreased, conductivity of YBCO film increases. Therefore at low temperatures YBCO film has high conductivity. Moreover, in these measurements the conductivity of gold film did not change with temperature. In addition to these, critical temperature of VO_2 film is found nearly at 340 K. Below the critical temperature VO_2 film is in the insulating state and it is transparent to THz radiation. However, above the critical temperature it blocked THz radiation because it is in the metallic state. This change in conductivity is also evident when examining the transmission using different substrates with the same patterned VO_2 film whereby an etalon effect was more pronounced for sapphire than fused silica allowing for the determination of the refractive index of these substrates.

Keywords: Superconductor, vanadium dioxide, conductivity, terahertz, THz-TDS, metamaterials, metasurface.

ÖZ

INCE FİLMLERİN İLETKENLİK OZELLİKLERİNİN TERAHERTZ BÖLGESİNDE KARAKTERİZASYONU

Akkaya, Merve
Yüksek Lisans, Fizik Bölümü
Tez Yöneticisi : Prof. Dr. Hakan Altan
Ortak Tez Yöneticisi : Doç. Dr. Cumali Sabah

August 2017, 63 sayfa

Terahertz bölgesinde ince filmlerin elektriksel ve optiksel karakterizasyonu hakkında neredeyse son otuz yıldır çalışılıyor.. Son birkaç yıldır terahertz bölgesinde optik elektronik alanında, vanadyum dioksit ve süperiletken gibi ince film üzerine çalışanlar için gelecek vaat edebilecek yeni bir dönemin kapıları açıldı. Vanadyum dioksitin ve süperiletkenlerin iletkenliği özellikle ilgi çekmektedir çünkü sıcaklık kritik sıcaklığın üzerine çıktığında vanadyum dioksitin iletkenliği değişmektedir ve aynı zamanda süperiletkenlerin de oda sıcaklığındaki iletkenliği düşük sıcaklıktaki iletkenliğinden farklıdır. Bu çalışmada yalıtkan yüzey üzerinde vanadyum dioksit ve süperiletken ince filmlerin iletkenliği laboratuarımızda geliştirilen ve katmanlı ortamların analitik ve nümerik modellemesi ile desteklenen spektroskopi sistemine dayalı deneysel metotlar kullanılarak incelenmiştir. Ek olarak, bu tip iletkenliği değiştirilebilen malzemeler, geçmişte büyük bir zorluk olan terahertz bölgesinde çalışabilen aletler geliştirmekte özel bir öneme sahiptir. Metamateryaller ve onların 2 boyutlu hali olan metayüzeyler bu boşluğu doldurmakta önemli bir role sahiptir. THz bölgesinde yttrium barium copper oxide (YBCO), altın ve vanadyum dioksit (VO_2) in iletkenlik özellikleri analiz edildikten sonra, çeşitli metayüzey modelleri Computer Simulation Technoloy (CST)

Microwave Studio kullanılarak simüle edilmiştir. Bu simülasyonlar materyallerin farklı iletkenlik özellikleri gösterdiği sıcaklıklarda yapılmıştır. Farklı sıcaklıklarda zamana dayalı spektroskopi yöntemleri kullanarak yapılan tek katmanlı YBCO, dörtlü çaprazlama yapılı işlenmiş altın ve YBCO film ve işlenmemiş VO_2 ölçümleri ile karşılaştırılmıştır. Sıcaklığı kontrol etmek için kriyostat kullanılmıştır. Sonuç olarak YBCO filmin kritik sıcaklığının 90K olduğu ve bu sıcaklığın altında metal gibi davrandığı ortaya çıkmıştır. Sıcaklık azaltıldığında YBCO filmin iletkenliğinin arttığı gözlemlenmiştir. Böylece düşük sıcaklıklarda YBCO filmin iletkenliğinin yüksektir. Altının iletkenliği sıcaklığa bağlı değildir. Bunlara ek olarak VO_2 filmin kritik sıcaklığı 340K yakınında bir değerdir ve kritik sıcaklığın altında yarıiletken durumdadır. Bu durumda THz radyasyonunu iyi geçirir. Ancak, kritik sıcaklığın üzerinde VO_2 film THz radyasyonunu engeller çünkü bu sıcaklık ve üzerinde VO_2 metalik duruma geçer. Farklı alt katmanlar kullanarak aynı yapıda işlenmiş VO_2 filmin geçirgenliğini incelediğimizde iletkenlikte ki bu değişiklik belirgindir. Etalon etkisinin safir alt katmanda kaynaşık silika alt katmana göre daha belirgin olması bu malzemelerin kırıcılık indisinin belirlenmesine olanak sağlar.

Anahtar Kelimeler: Süperiletkenler, vanadyum dioksit, iletkenlik, terahertz, THz-TDS, metamalzeme, metayüzey.

To My Dear Family

ACKNOWLEDGEMENTS

First and foremost, I would like to thank to my supervisor Prof. Dr. Hakan Altan, Prof. Dr. Lütfi Özyüzer and Assoc. Prof. Dr. Cumali Sabah for their support knowledge and guidance during my study.

I wish to thank all members of METU Terahertz Research Laboratory: Burcu Karagöz, Namıg Alasgarzade, Mehmet Ali Nebioğlu, Ümit Alkuş, İhsan Ozan Yıldırım, Taylan Takan, Hakan Keskin for their contributions to this study.

I am also thank to colleagues in IZTECH Terahertz Laboratory for samples especially Yasemin Demirhan.

I owe my hearty thanks to Nevra Akalın, Hazal Doğaroğlu, Gilda Afshari, Ece Alaçakır, Fırat Yalçın for their endless support, cooperation, helping me in all the possible ways and for being amazing friends.

I would like to express my deepest thanks and love to my family who always offered their unconditional love, care and support during all my life.

I would also like to acknowledge the support provided by The Scientific and Technological Research Council of Turkey (TUBITAK) Grant # 115F226 and # 114F379.

TABLE OF CONTENTS

LIST OF TABLES

TABLES

LIST OF FIGURES

FIGURES

LIST OF ABBREVIATIONS

THz	Terahertz
EM	Electromagnetic
TDS	Time Domain Spectroscopy
SLM	Spatial Light Modulator
MMA	Metamateial Absorber
OR	Optical Rectification
PCA	Photoconductive Antenna
fs	femtosecond
FTIR	Fourier Transform Infrared Spectroscopy
YBCO	Ytrrium Barrium Copper Oxide
HT_C	High Temperature
CST-MW-Studio	Computer Simulation Technology-Microwave Studio
E-field	Electric Field
nm	nanometer (10^{-9} m)
AC	Alternating Current
DC	Direct Current
ps	picosecond
µm	micrometer (10^{-6} m)

CHAPTER 1

INTRODUCTION

Materials which have tunable temperature dependent conductivity such as YBCO, and VO_2 have taken attention since they can be used in devices that can control the interaction of terahertz (THz) waves. In order to better understand and better implement them, the conductive properties of YBCO, gold and VO_2 films are investigated in the THz region at different temperatures. After investigating the critical transition temperatures of YBCO and VO_2 films, different patterned metasurface structures were studied to investigate both the temperature dependence of resonance frequencies and dependence of bandpass effects on the conductivity of the film.

One type of electromagnetic radiation is THz radiation and the region between Microwave and Infrared region called as Terahertz frequency range. Also, it corresponds to 10^{12} Hertz in the electromagnetic (EM) spectrum. Therefore, it is in the region between 10^{11} and 10^{13} Hertz. This THz radiation waves called as T-rays have the following characteristics at 1 THz in free space :

- Energy of the photon : 4.1 meV $(E = hf)$
- Temperature : 48 K $(T = hf/k_B)$
- Wavelength : 300 μm $(\lambda = c/f)$
- Period : 1 ps $(\tau = 1/f)$
- Wave number : 33.3 cm^{-1} $(\bar{k} = 1/\lambda)$

where h is the Planck's constant, f is the frequency, k_B is the Boltzmann's constant and c is the speed of light [1].

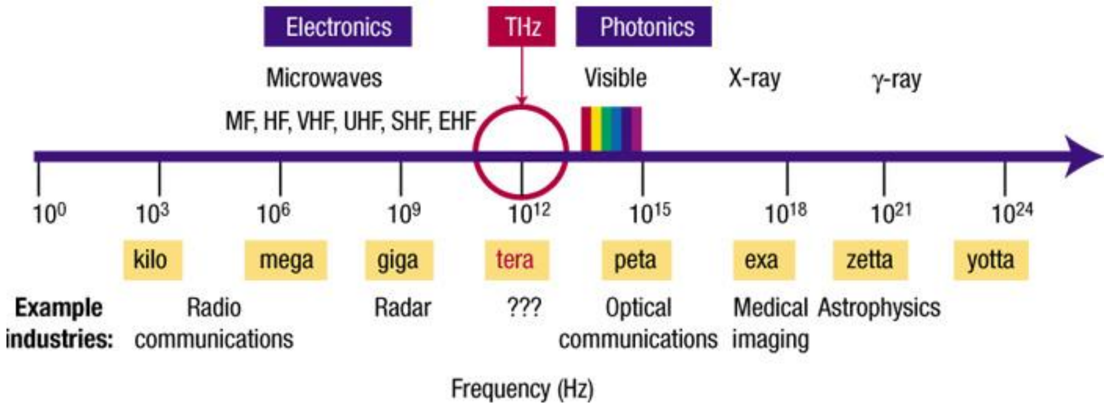

Figure 1.1 : THz region in the electromagnetic spectrum. This Figure is adapted from [2].

THz band reaches over the frequencies between 0.3 THz and 10 THz [3]. In the microwave region of the electromagnetic spectrum, there are countless applications in the area of electronics and also infrared region is considered to have applications in photonics. Therefore, these two technologies are significant to generate and detect THz radiation.

Generally, THz range of the electromagnetic spectrum known as "THz Gap" [1]. Although, there are lots of methods to generate and detect electromagnetic radiation at nearly every frequency, due to difficulties associated with the energy and generation/detection of the radiation most of the THz region has not been explored [4].

In THz region it is important to develop technologies which can both tune frequency and amplitude or intensity of THz radiation. At room temperature it has been a challenging issue to develop devices which can work in this frequency range since these photons have low energy. Recent studies suggest frequency selective surfaces and metamaterials offer a new way in the interested frequency range to manipulate reflection or transmission of THz waves. Therefore, metamaterials play an important role to fill the THz gap [5]. In order to control electromagnetic radiation metamaterials are designed and they are man-made sub-wavelength composite structures [6]. Metamaterials have structural periodic units. Effective medium theory, which explains the behavior of a composite structure, has a significant role in modeling metamaterials. According to effective medium theory, since metamaterials are sub-wavelength structures, scales of unit cell dimensions of matematerial and scales of structural unit spacing of metamaterials should be in the sub-wavelength region [7]. Moreover, two dimensional type of metamaterials are called as metasurfaces. Different from metamaterials, conductive layer thickness should not be zero in metasurfaces. Furthermore, effective medium theory also used to model metasurfaces. Sometimes instead of using metamaterials, metasurfaces are used because they take up less space as compared to metamaterials [8]. As a result less lossy structures can be made by using metasurfaces. Since metamaterials are generally characterized as a medium which exhibits a negative refractive index, the drawback with metasurfaces is that it is difficult to obtain this effect when the THz radiation is incident perpendicularly to the plane.

One of the most important applications of THz technology is development of terahertz time domain spectroscopy (TDS) techniques [9]. This spectroscopic technique is used for the characterization of materials especially dielectrics, semiconductors and also characterization of superconductors can be done with this system. This system is used not only in research laboratories but also this system can be used in the area of industrial and metrology applications [10]. By using this system it is possible to find refractive index, power absorption and also conductivity of thin films.

Some materials show different conductive properties at different temperatures in THz frequency range. Superconductors and metal-insulator transition materials are those kinds of materials [11]. Their conductive properties can change as a function of the temperature. Therefore, their transmissive properties are also affected by this change.

1.1 Applications of Metasurfaces

Metasurfaces or metamaterials shows different properties and this properties aid scientist or engineers to develop high performance terahertz devices [12]. There are lots of applications of metasurfaces in THz region. It can be used in the area of imaging, for sensor applications and modulators.

1.1.1 Imaging Applications of Metasurfaces

In recent year imaging application in THz frequency band took attention by offering inspiring opportunities. Ultrathin flat metasurface lenses are one of fascinating application of metasurfaces in THz region on the area of imaging and lensing. According to research which is published in 2014, flat metasurface lenses were designed. Structure of this lens enables high transmission in a broad terahertz band. Also these flat lenses are useful for reducing spherical aberration, coma and other aberrations [13].

This structure includes thin dielectric spacer and on two sides of this spacer there are slotted metallic resonators [14]. Spatial distribution of the THz field is controlled by altering the geometrical parameters in Figure 1.2. According to their research it is investigated that this design shows high transmission and strong focusing at the frequency region of interest.

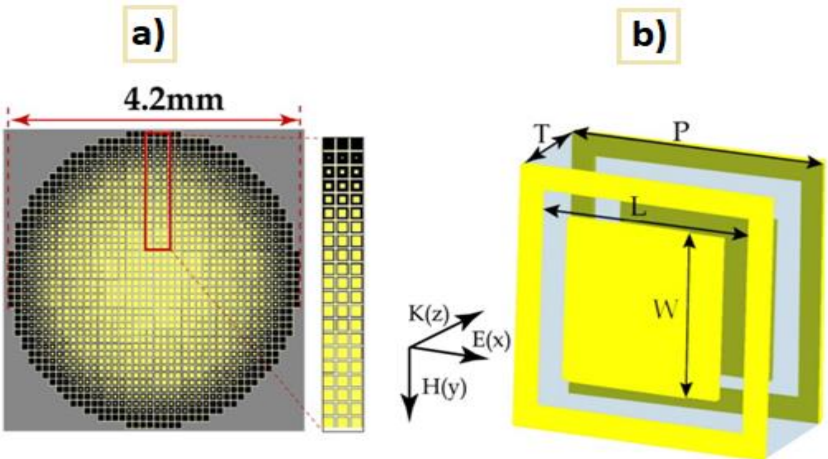

Figure 1.2: a) front view of terahertz metasurface lens b) Structure of terahertz metasurface lens. This Figure is adapted from [14].

1.1.2 Sensor Applications of Metasurfaces

Many diseases are because of microorganisms such as bacteria and fungi. To prevent and detect infections which is caused by bacteria or fungi it is important to develop fast and correct techniques. In terahertz region it is possible to detect microorganisms with metasurfaces since scales of micro gaps in metasurfaces and microorganisms are in agreement with each other. In 2013, there is published research about this issue [15]. In this research penicillin is observed by using electrical resonator. Taken in consideration of the size of the biological element, structure of metamaterial can be created. By using this method detection becomes fast as compared to contemporary microbial detection techniques.

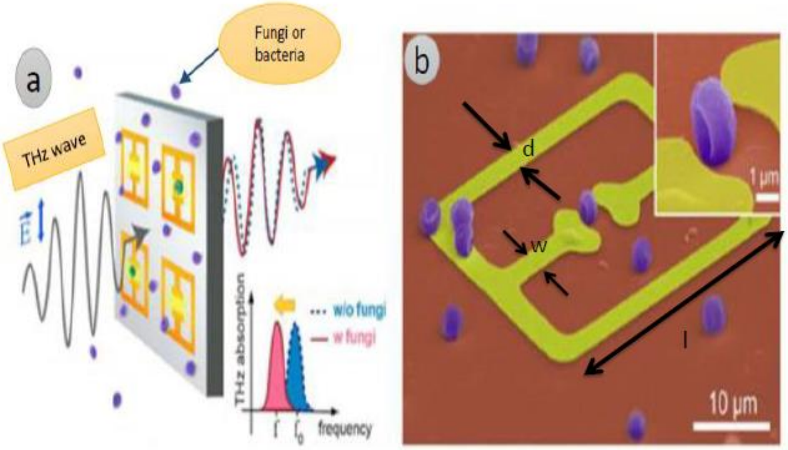

Figure 1.3: a) Shematic representation of THz metamaterial for the use of sensing b)Scanning microscope image of this strucutre. This Figure is adapted from [15].

1.1.3 Modulator Applications of Metasurfaces

Modulation of light is a fundamental operation in photonics. By tuning metamaterials' electromagnetic properties with numerous mechanisms, it is possible to made to be both spatially and frequency selective [16]. In 2013 Padilla and his group published their work on a doped semiconducting metamaterial spatial light modulator (SLM) work [16]. It has multi-color super-pixels and it consists of arrays. In Figure 1.4 photograph of implementation of 8×8 pixel metamaterial absorber (MMA) spatial ligth modulator and microscpope images of each color pixel is shown. Density in high pixels and minimum device capacitance are achieved by using a flip-chip bonded n-doped epitaxial layer of gallium arsenide [16]. Therefore, high speed modulation is also obtained.

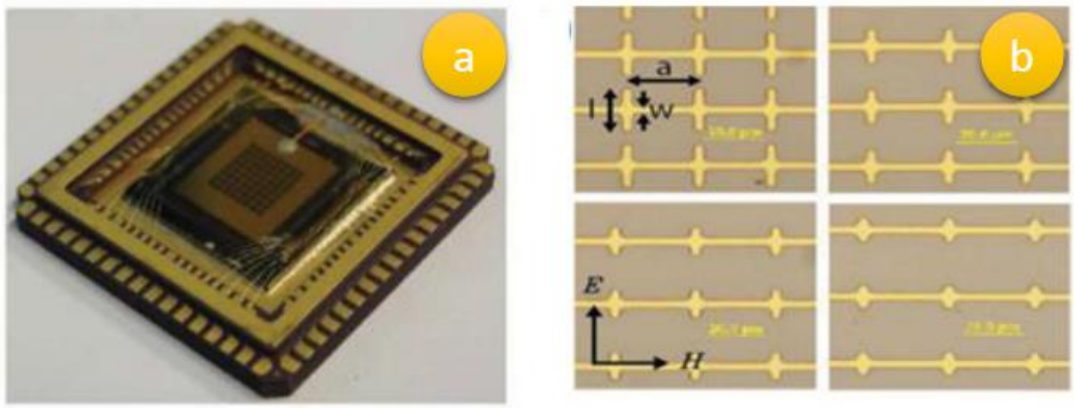

Figure 1.4: (a) Design and structure of THz metamaterial absorber which based SLM (b) Optical microscope image of each pixel color. This Figure is adapted from [16].

Also, different thin films are used in terahertz region. In this study, VO_2 is used and there are several applications of this film in terahertz region. For example, bolometers, tunable filters and spectroscopy devices are potential applications of VO_2 film since its phase can change easily from insulator to metal. As an example of applications of this film bolometers are used in detection of electromagnetic radiation and also detection of heat. Therefore, bolometers can be used in thermal cameras, in detection of forest fire etc.

CHAPTER 2

PRINCIPLES OF TERAHERTZ SPECTROSCOPY

2.1 Terahertz Generation

Terahertz generation can be separated into two parts: continuous and pulsed wave generation. In this study, only pulsed wave generation was considered. In THz time domain spectroscopy (THz-TDS) systems, generation of pulsed THz waves is based on optical rectification (OR) methods and/or photoconductive antenna (PCA) devices.

2.1.1 Optical Rectification

This method is second order nonlinear optical technique for generation of THz pulse [17]. It produces a quasi-DC polarization in a nonlinear medium (crystal) by getting through an intense beam of light. Also, electro optic sampling is the reverse process of this phenomenon. Generation of the THz pulse with the optical rectification depends on the combining different frequency components [4]. However, there are several factors that can affect the efficiency of radiation, waveform and frequency bandwidth. These factors can be absorption and dispersion, crystal thickness, phase matching and diffraction [4].

When femtosecond (fs) pulses focused on nonlinear medium, materials have second order susceptibility and it is different from zero. Zinc Telluride (ZnTe), Gallium Phosphide (GaP) and Gallium Selenide (GaSe) are examples of these materials [18].

Electric field affect the polarization state of these materials. Power series can be used to model susceptibility and in this model second and higher order polarizability terms are nonlinearly proportional to applied electric field. Laser pulse have different frequencies and photons interacts with each other at different frequencies. Therefore, this situation results in having frequency dependent polarization.

$$\vec{P} = \varepsilon_0 \vec{E}[\chi^{(1)} + \chi^{(2)}\vec{E} + \chi^{(3)}\vec{E}\vec{E} + \cdots] \tag{2.1}$$

where $\vec{P}$ is the induced polarization, $\chi^{(n)}$ is nth order susceptibility tensor and ε_0 is the permittivity in vacuum.

Result of the optical rectification is in the second term of the Eq. (2.1). Therefore polarization because of optical rectification can be demonstrated as

$$P_X^{(2)} = \sum_{j,k} \varepsilon_0 \chi_{ijk}^{(2)} E_j(w) E_k^*(w) \qquad \text{i, j, k=1, 2, 3} \tag{2.2}$$

where i, j and k represents Cartesian coordinates and $\chi^{(2)}$ is second order susceptibility.

The amplitude of THz field and second derivative of polarization with respect to time related with each other as stated below

$$\vec{E}_{THz} \propto \frac{\partial^2 \vec{P}}{\partial t^2} \tag{2.3}$$

In order to have broadband THz pulse optical rectification method can be used and having broad spectral bandwidth is unique advantage of this method [4].

2.1.2 Photoconductive Antenna

One of the fundamental device for generation of Terahertz pulse is photoconductive antenna (PCA). A PCA have two metal electrodes and these electrodes are deposited on a semiconductor substrate. Radiation damaged Silicon-on-Sapphire (RD-SOS), low temperature grown Gallium Arsenide (LT-GaAs), Indium Phosphide (InP) are the examples of most commonly used substrates to generate THz radiation [4].

PCA acts like a switch. In the determination of operation cycle of the switch the most significant factor is the optical pulse. After the laser pulse illuminates the gap of antenna, electron hole pair and photo induced carriers are generated. However in order to generate electron hole pair the energy of the laser pulse must be greater than the energy gap of the semiconductor substrate. Applying electrical bias to the metal plate help by generating electrical field and then generating photocurrent. Photocurrent is expressed as

$$\vec{J}(t) = e\mu N(t)\vec{E}_b \tag{2.4}$$

where μ is carriers mobility, e is charge of the electron and N photoinduced carriers density and E_b is the biased electric field.

THz wave is generated by the rapid change in this current and its electric field is described as

$$\vec{E}_{THz} = \frac{A}{4\pi\varepsilon_0}\frac{1}{zc^2}\frac{\partial\vec{J}(t)}{\partial t} \tag{2.5}$$

where A is the illuminated area, z is the penetration distance of the incoming beam into the semiconducting substrate and c is the speed of light in vacuum.

Thus the THz pulse amplitude is proportional to time derivative of photocurrent.

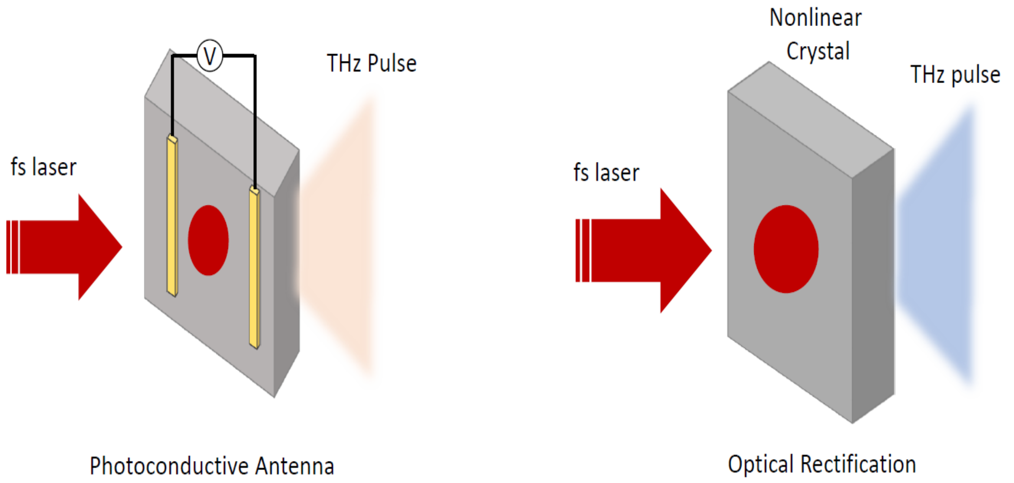

Figure 2.1: Schematic representation of THz pulse generation methods.

2.2 Terahertz Detection

In THz time domain spectroscopy systems, detection of pulsed THz wave is generally based on PCA and/or electro optic effect (EO).

2.2.1 Electro Optic Effect

Reverse process of generation of THz pulse by optical rectification is electro optic effect as expressed in the generation part. Optical rectification and electro optic effect rely on Pockels effect and both of them are nonlinear effects [19]. Depending on the applied electric field, refractive index of the nonlinear crystal or birefringence changes and this effect known as Pockels effect [20]. Changing the refractive index of the crystal results in the probe beam modulation. Both THz pulse and fs laser probe beam propagates in the crystal. As a result of this co-propagation linearly polarized laser pulse changes into elliptically polarized whose components are analyzed. Furthermore, when linearly polarized light propagates through the crystal without THz pulse, the optical components used to analyze the intensity of the polarization components of the probe beam is selected such that the linearly polarized beam becomes circularly polarized to ensure a balance between the respective components.

These optical components are comprised of a quarter wave plate as well as a Wollaston prism, where the elliptically polarized beam‘s perpendicular components are divided into two parts. Intensity difference of these pulses are measured by a pair of photodiodes. If the THz pulse is not on the EO crystal, the components have equal intensity due to the quarter wave plate and there is no signal difference to measure on the detector. On the contrary, if THz pulse is focused onto the EO crystal, the detector measures a difference signal and this signal is proportional to THz pulse electric field.

2.2.2 Detection with Photoconductive Antenna

The PCA can also be used for the detection of THz pulses. However, there is difference between generation and the detection of THz pulse with PCA. In the detection process bias voltage is not applied to the transmission line. When antenna receive the optical pulse in the valance and the conduction band electron-hole pairs are generated. Then, THz wave act as bias voltage. Photoconductive current is generated by THz pulse and by the measurement of current between optical pulse and THz pulse time delay the form of the THz pulse is determined.

Figure 2.2: Schematic representation of detection of THz pulse with electro optic

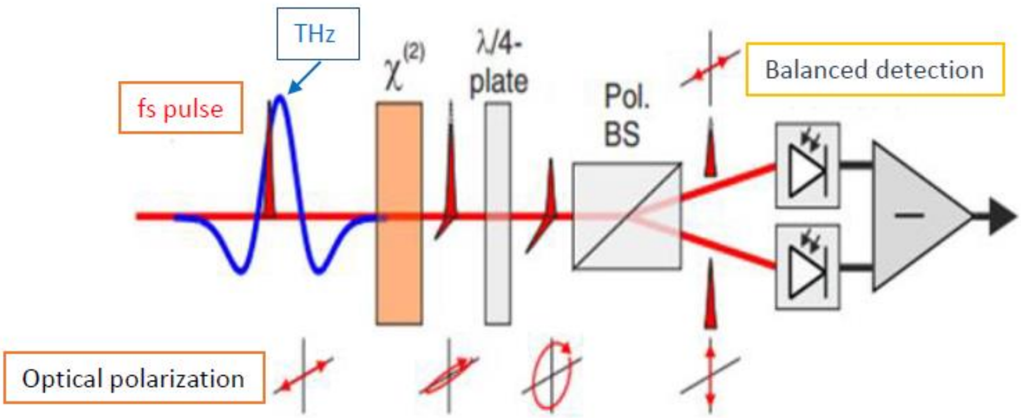

effect. This Figure is adapted from [21].

2.3 Terahertz Time Domain Spectroscopy

In this study THz-TDS is used to characterize samples. This system uses PCA in generation and EO sampling in detection. A femtosecond Ti:Sapphire mode-lock laser which has 75 MHz repetition rate with 800 nm central wavelength and 16 fs pulse width used as light source driving this system. Also, this system has several optical and electrical components. Function generator, power supply, lock in amplifier, antenna, balanced photodiode, lenses, filters, wave plates, mirrors and prism are examples of these components.

In this system output laser beam is divided into the generation and the detection arm by using beam splitter with transmission ratio of 95:5. Commercially obtained PCA generates the THz radiation and this PCA is modulated at 1 kHz with bias +/- 15 V. Then the generated radiation is collected with the help of a silicon lens, the THz waves scattered through the off axis parabolic mirror. Converging TPX lens is used to focus THz radiation on to the sample so efficient sample-THz interaction is obtained. Afterwards, diverging THz beam is collimated with another TPX lens. Next, another off axis parabolic mirror is used to collect and focus this beam onto the ZnTe crystal.

In the detection arm there is a corner cube on the top of the translational stage it is used for scanning the THz waveform electric field. The beam in the detection arm is directed onto the corner cube. The stage is moved step by step through the waveform and then THz waveform is gathered. Moreover, the whole system is controlled by a computer. Polarization of the fs visible pulse alters when it passes through the electro optic set up for different values of electric field of THz. In some measurements which the temperature of the sample is not changed plexiglass box is used to eliminate the effect of dust and nitrogen (N_2) gas is given into the box to reduce the humidity in the measurement. In Figure 2.3 THz-TDS system is shown in schematic view.

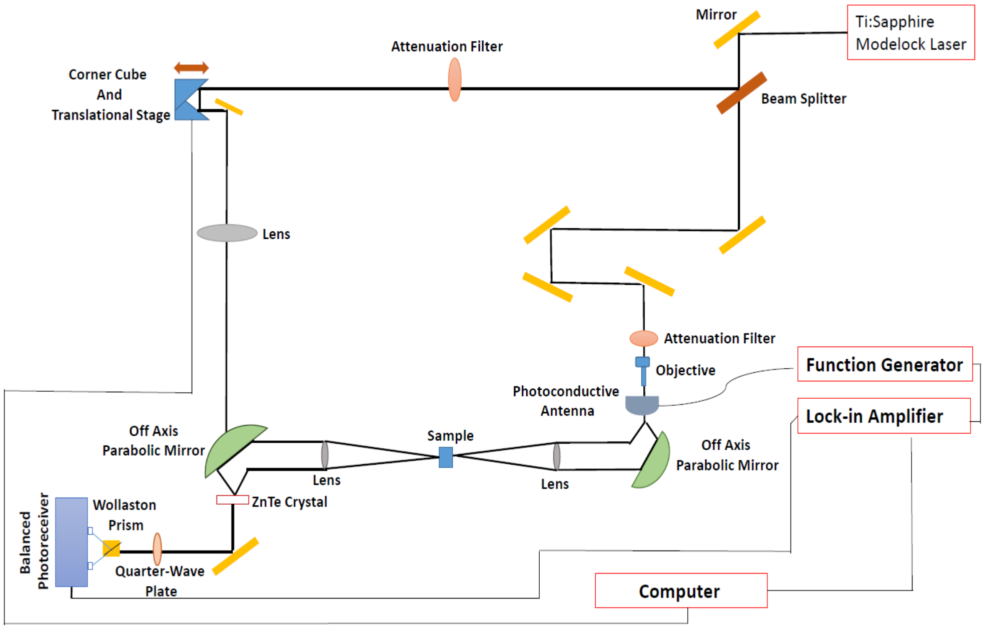

Figure 2.3: Schematic view of the THz-TDS system.

2.3.1 Data Analysis

In THz-TDS system intensity and also electric field measurements can be measured. Fourier transform infrared spectroscopy (FTIR) is another spectroscopic method in far infrared region. However, using THz-TDS system is more advantageous than FTIR since phase change in measurements can be detected by only THz-TDS. In THz-TDS system measurement of electric field of THz pulse allows retrieval of phase information and amplitude where after the complex refractive index of sample and effective dielectric constant of the sample can be found.

From the THz-TDS measurements, firstly THz electric field with respect to time is obtained. Then with the help of a Fast Fourier Transform (FFT), THz electric field can be calculated as a function of frequency as seen in Figure 2.4 and then in the frequency domain THz electric field can be expressed

$$E(z,\omega) = \frac{1}{\sqrt{2\pi}} \int_{-\infty}^{+\infty} E(z,t)\, e^{-i\omega t} dt \tag{2.6}$$

Then,

$$E(z,\omega) = A(z,\omega)e^{-i\varphi(\omega)} \tag{2.7}$$

where amplitude of the electric field is $A(z,\omega)$, $\varphi(\omega)$ is electric field phase and here $\omega = 2\pi f$ and ω is angular frequency and f is the frequency. Thus, in Eq. (2.7) both amplitude and phase information can be obtained by THz-TDS system.

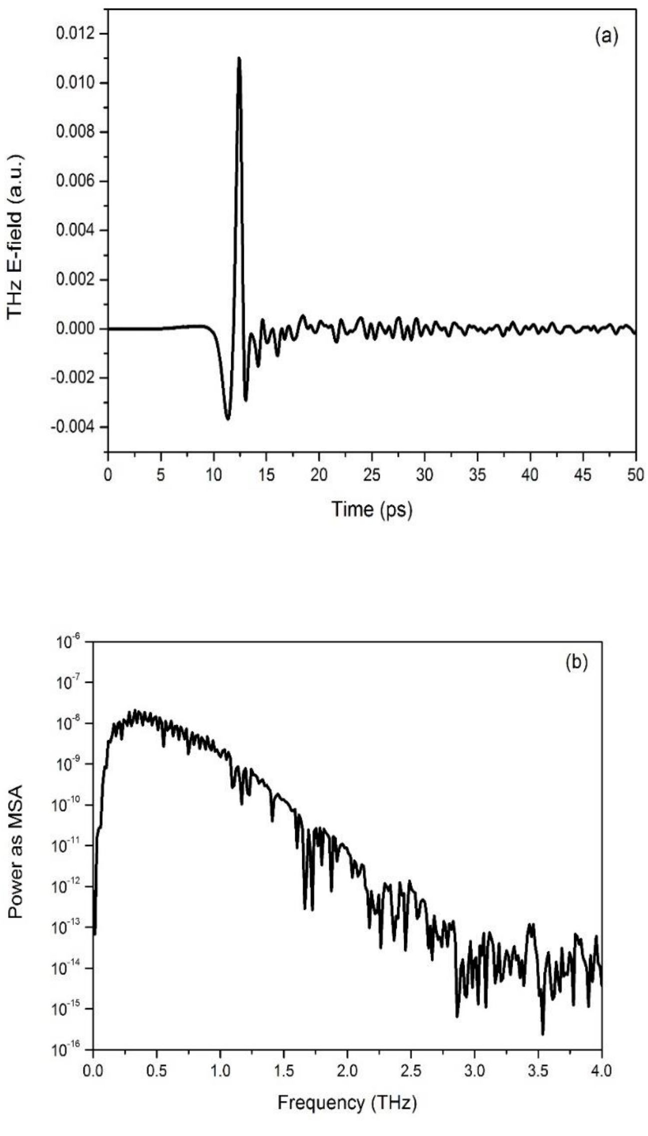

Figure 2.4: (a) THz pulse electric field in time domain. (b) Power spectrum of the pulse after Fourier transform in frequency domain.

After phase and amplitude information obtained in the frequency domain from Fourier transform, refractive index and power absorption of the sample can be calculated as [22]

$$n(\omega) = 1 + \frac{c}{2\pi f d}(\varphi_{samp}(\omega) - \varphi_{ref}(\omega)) \tag{2.8}$$

$$Power\ Abs = \frac{-1}{d}\ln\left(\frac{Power_{samp}}{Power_{ref}}\right) \tag{2.9}$$

where refractive index of sample is n, c is speed of light in vacuum, φ is phase of the sample and reference in radian, d is the sample thickness.

Complex refractive index of the sample can be written in the form of

$$\tilde{n} = n(\omega) + ik(\omega) \tag{2.10}$$

where $k(\omega)$ is extinction coefficient and it is expressed as

$$k(\omega) = \frac{\alpha(\omega)c}{2\omega} \tag{2.11}$$

where $\alpha(\omega)$ is absorption coefficient and c is the speed of light in vacuum.

Therefore complex dielectric function can be calculated through this formula

$$\varepsilon(\omega) = \varepsilon_R(\omega) + i\varepsilon_I(\omega) \tag{2.12}$$

$$\varepsilon(\omega) = \tilde{n}^2 \tag{2.13}$$

$$\varepsilon_R = n^2(\omega) - k^2(\omega) \quad \text{and} \quad \varepsilon_I = 2n(\omega)k(\omega) \tag{2.14}$$

2.4 Fresnel Coefficients and Transfer Matrix Method

In the optical medium electromagnetic waves propagation can be defined by four Maxwell equation [23]. Boundary conditions of a linear dielectric medium where electric and magnetic field incident on can be expressed as

$$E_1^{\parallel} = E_2^{\parallel} \tag{2.15}$$

$$\epsilon_1 E_1^{\perp} = \epsilon_2 E_2^{\perp} \tag{2.16}$$

$$\frac{1}{\mu_1} B_1^{\parallel} = \frac{1}{\mu_2} B_2^{\parallel} \tag{2.17}$$

$$B_1^{\perp} = B_2^{\perp} \tag{2.18}$$

These equations are the fundamental for reflection and refraction theory at optical interfaces. There are two type of polarization and it relies on the direction of the electric field. When the electric field of the incident wave is parallel to the plane of incidence it is called as p-polarized and if electric field of the incident wave is perpendicular to the plane of incidence it is described as s-polarized [24]. In Figure 2.5 different type of polarization can be seen. In this figure blue color represents the electric field which lies in the plane of incidence in p-polarization and red color represents the magnetic field which lies in the plane of incidence in s-polarization.

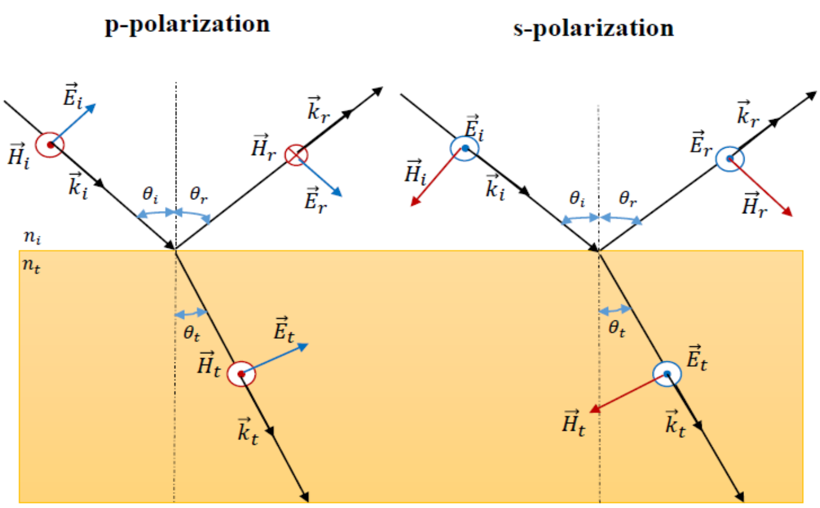

Figure 2.5: Reflection and refraction for p and s polarization.

In Figure 2.5 subscripts *i*, *r* and *t* means incident transmitted and reflected and also $\vec{k}$ is the propagation vector, $\vec{E}$ is electric field vector and $\vec{B}$ is magnetic field vector. Moreover, θ_i, θ_r and θ_t are the angle of incidence, angle of reflection and angle of transmission, respectively. Relation between these angles can be expressed as

$$\theta_i = \theta_r \tag{2.19}$$

$$n_i sin\theta_i = n_t sin\theta_t \tag{2.20}$$

This relation called as Snell's law. Also Fresnel coefficients can be derived by using Eq. 2.15 and Eq. 2.17. Therefore, Fresnel coefficients can be expressed as

$$r^s = \frac{E_r^s}{E_i^s} = \frac{n_i cos\theta_i - n_t cos\theta_t}{n_i cos\theta_i + n_t cos\theta_t} \tag{2.21}$$

$$t^s = \frac{E_t^s}{E_i^s} = \frac{2n_i cos\theta_i}{n_i cos\theta_i + n_t cos\theta_t} \tag{2.22}$$

$$r^p = \frac{E_r^p}{E_i^p} = \frac{n_t cos\theta_i - n_i cos\theta_t}{n_t cos\theta_i + n_i cos\theta_t} \tag{2.23}$$

$$t^p = \frac{E_t^p}{E_i^p} = \frac{2n_i cos\theta_i}{n_t cos\theta_i + n_i cos\theta_t} \tag{2.24}$$

where r^s and r^p are reflection coefficient for perpendicularly and parallel polarized light respectively, t^s and t^p are transmission coefficient for perpendicularly and parallel polarized light. In addition, transmitted and reflected power defined as

$$R = |r|^2 \tag{2.25}$$

$$T = \frac{n_t}{n_i} |t|^2 \tag{2.26}$$

Transfer matrix method aid us to calculate optical response of a layer sequence of thin films. This method use a characteristic matrix and electric and magnetic field is correlated at both interfaces of an optical medium [25], [26]. For example, when single layer is used, this layer is in between two media and assume that optical thickness of this media is *d*. Therefore, sequence of thin films are media 0- layer 1- media 2. Also according to the boundary conditions in Eq. 2.15-2.18 for at interface 01:

$$E_{0i} + E_{0r} = E_{1i} + E_{1r} \tag{2.27}$$

$$n_0 E_{0i} - n_0 E_{0r} = n_1 E_{1i} - n_1 E_{1r} \tag{2.28}$$

For at interface 12:

$$E_{1i} e^{ikd} + E_{1r} e^{-ikd} = E_t \tag{2.39}$$

$$n_1 E_{1i} e^{ikd} - n_1 E_{1r} e^{-ikd} = n_2 E_t \tag{2.40}$$

From the combination of these equations

$$1 + \frac{E_{0r}}{E_{0i}} = \frac{E_t}{E_{0i}} \left(coskd - i \frac{n_2}{n_1} sinkd \right) \tag{2.41}$$

$$n_0 - n_0 \frac{E_{0r}}{E_{0i}} = \frac{E_t}{E_{0i}} (-i n_1 sinkd + n_2 coskd) \tag{2.42}$$

Also, these equations can be written in the matrix form

$$\begin{pmatrix} 1 \\ n_0 \end{pmatrix} + \begin{pmatrix} 1 \\ -n_0 \end{pmatrix} \frac{E_{0r}}{E_{0i}} = \begin{pmatrix} coskd & \left(-\frac{i}{n_1}\right) sinkd \\ -i n_1 sinkd & coskd \end{pmatrix} \begin{pmatrix} 1 \\ n_2 \end{pmatrix} \frac{E_t}{E_{0i}} \tag{2.43}$$

Moreover, this equation can be written in that form

$$\begin{pmatrix} 1 \\ n_0 \end{pmatrix} + \begin{pmatrix} 1 \\ -n_0 \end{pmatrix} r = P \begin{pmatrix} 1 \\ n_2 \end{pmatrix} t \tag{2.44}$$

where P is transfer matrix, *t* is transmission coefficient and *r* is reflection coefficient. Therefore this formula can be extended for multiple layers,

$$\begin{pmatrix} 1 \\ n_0 \end{pmatrix} + \begin{pmatrix} 1 \\ -n_0 \end{pmatrix} r = P_1 P_2 P_3 \ldots P_N \begin{pmatrix} 1 \\ n_2 \end{pmatrix} t \tag{2.45}$$

$$\begin{pmatrix} 1 \\ n_0 \end{pmatrix} + \begin{pmatrix} 1 \\ -n_0 \end{pmatrix} r = P_{total} \begin{pmatrix} 1 \\ n_2 \end{pmatrix} t \tag{2.46}$$

where P_{total} is product of transfer matrices.

2.4.1 Analysis of Single Slab

In this study, layered structures were used and these structures have dielectric substrates such as sapphire and fused silica. It is important to use a substrate which is transparent for the THz pulse to investigate the conductive properties of sample. In order to find effect of substrate, extracted and the measured results are compared and this calculation is made for quartz substrate. Therefore, transmission and reflection coefficients are known from Eq. 2.21- 2.24. These equations can be written in that form

$$R_{12}(\omega) = \frac{n1\,(\omega) - n_2(\omega)}{n_1(\omega) + n_2(\omega)} \tag{2.47}$$

$$T_{12}(\omega) = \frac{2 * n_1(\omega)}{n_1(\omega) + n_2(\omega)} \tag{2.48}$$

$$R_{21}(\omega) = \frac{n2\,(\omega) - n_1(\omega)}{n_1(\omega) + n_2(\omega)} \tag{2.49}$$

$$T_{21}(\omega) = \frac{2 * n2\,(\omega)}{n_1(\omega) + n_2(\omega)} \tag{2.50}$$

When wave propagates in medium 1, it moves into the interface of medium 1-2 and then it is reflected back to medium 1 and it corresponds to R_{12}. Also, transmission occurs from medium 1 to medium 2, so it is called T_{12}. Therefore, there is a two route for the transmitting wave, one of them is reflection at interface 2-1 and it is called R_{21} and other is transmission into medium 1 and it is called as T_{21}.

Also, it is known that total transmission coefficient is

$$t(\omega) = \sum_j T_{12}(\omega) * P_2(\omega, d) * [R_{12}(\omega) * P_{12}(\omega, d) * R_{21}(\omega)]^j * T_{21}(\omega) \tag{2.51}$$

In that form it is difficult to calculate *t(ω)*. Therefore by using the following relations Eq.2.52 and Eq. 2.53 calculation of total transmission coefficient becomes easier.

$$\sum_{j} \mathrm{P}_2(\omega, \mathrm{d}) * [R_{12}(\omega) * P_{12}(\omega, d) * R_{21}(\omega)]^j = \frac{1}{1-\left(\frac{n2\,(\omega)-n_1(\omega)}{n_1(\omega)+n_2(\omega)}\right)^2 * P_2^2(\omega, d)} \tag{2.52}$$

$$P_2(\omega) = e^{i*n_2(\omega)*d*\omega/c} \tag{2.53}$$

Then, Eq.2.51 can be expressed as

$$t(\omega) = \frac{2*n_1(\omega)}{n_1(\omega)+n_2(\omega)} * \frac{1}{1-\left(\frac{n2\,(\omega)-n_1(\omega)}{n_1(\omega)+n_2(\omega)}\right)^2 * e^{2*i*n_2(\omega)*d*\frac{\omega}{c}}} * \frac{2*n_2(\omega)}{n_1(\omega)+n_2(\omega)} \tag{2.54}$$

where n_1 and n_2 are refractive index of air and quartz respectively, d is the thickness of quartz and w is the frequency and c is the speed of light in vacuum. Here refractive index of air is 1 and n_2 can be calculated from Eq. 2.8.

After the calculation of total transmission coefficient, by using following equation extracted value of complex electric field of quartz *E(ω)* can be calculated

$$t(\omega) = \frac{E(\omega)}{E_0(\omega)} \tag{2.55}$$

where E_0 is measured air reference. Moreover, power magnitude and power MSA of extracted value for *E(ω)* can be calculated. Then the comparison between extracted result and measured result of power MSA can be shown in Figure 2.6.

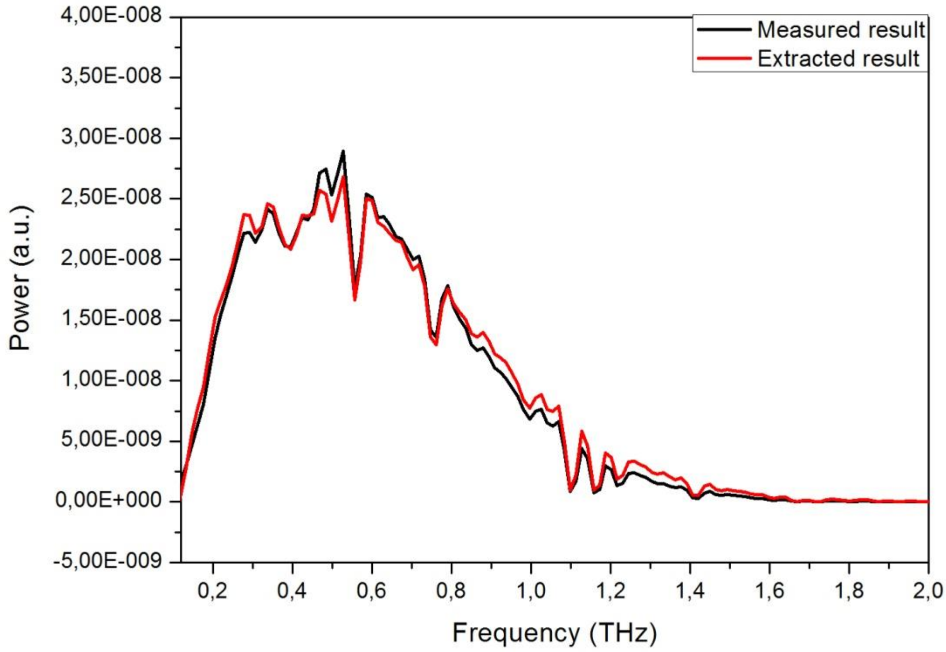

Figure 2.6: Power spectrum of the THz pulse for extracted and measured results of power MSA values. Extracted result was obtained by multiplying the reference measurement with calculated Fresnel transmission coefficient for the quartz substrate.

2.5 Effect of Conductivity

Bulk conductivity of materials depends on refractive index and extinction coefficient of the materials. Therefore, refractive index of the material and also extinction coefficient of the materials should be known to find the bulk conductivity of the material. Real and imaginary part of the bulk conductivity is expressed as

$$\sigma_R = 4\pi\varepsilon_0 f\ n\ (c\frac{PowerAbs}{4\pi f}) \tag{2.56}$$

$$\sigma_I = [\varepsilon_b - n^2 + (c\frac{PowerAbs}{4\pi f})^2]\varepsilon_0 2\pi f \tag{2.57}$$

where n is refractive index of material, f is the frequency, c is speed of light in vacuum, ε_0 is permittivity in vacuum and generally $\varepsilon_b = n^2$.

There is another way for calculating conductivity. In this way, refractive index and extinction coefficient not need to be known to calculate conductivity. Eq. 2.58 comes from Tinkham formula [27] by using boundary conditions on electric and magnetic fields, Fresnel coefficients for transmission and some manipulations on Fresnel coefficients Tinkham formula is obtained. As a result, field transmission and thin film complex conductivity are associated. However, this method is suitable for very thin layers and it gives sheet conductivity. Heinz *et al.* used this method to calculate sheet conductivity of graphene monolayer which is complex [28]. In this model frequency dependent electric fields were used and relation between conductivity and electric fields are expressed as

$$\frac{E(\omega)}{E_0(\omega)} = \frac{n+1}{n+1+Z_0\sigma_{sheet}(\omega)} \tag{2.58}$$

where Z_0 is impedance of free space, n is refractive index of substrate, E is complex electric field of the graphene monolayer, E_0 is complex electric field of the substrate.

Therefore, when this formula was adapted to the vanadium dioxide (VO_2) on dielectric sapphire substrate, E became the complex electric field of VO_2 and E_0 is complex electric field of sapphire substrate.

Therefore sheet conductivity can be expressed as

$$\sigma_{sheet}(\omega) = \frac{(n+1)(E_0(\omega)-E(\omega))}{E(\omega)Z_0} \tag{2.59}$$

There is a relation between sheet conductivity and conductivity of thin films. When sheet conductivity is divided into thickness of VO_2 film, complex conductivity of VO_2 film can be obtained [29], [30]. Therefore Eq.2.58 can be transformed into

$$\frac{E(\omega)}{E_0(\omega)} = \frac{n+1}{n+1+Z_0\sigma(\omega)d} \tag{2.60}$$

Then Eq.2.59 also transformed into

$$\sigma(\omega) = \frac{(n+1)(E_0(\omega)-E(\omega))}{E(\omega)Z_0 d} \tag{2.61}$$

where d is the thickness of thin film.

In commercially available programs, information about some materials such as VO_2 and yttrium barium copper oxide (YBCO) are not included. Thus, these kind of materials can be modelled in CST-Microwave Studio by using surface impedance table [31], [32]. In this table, surface resistance and reactance values which depend on frequency should be known. Therefore surface impedance can be expressed as

$$Z_s = R_s + iX_s \tag{2.62}$$

$$Z_s = \sqrt{\frac{i\omega\mu_0}{\sigma}} \coth(d\sqrt{i\omega\mu_0\sigma}) \tag{2.63}$$

where R_s stands for surface resistance and X_s signifies surface reactance and d is thin film thickness.

2.6 Closed Cycle Cryostat

Closed cycle cryostat obtained from the Solar Energy Research Center at METU, Ankara (GUNAM) was used to control the temperature during the measurements. The system used for the purpose of cooling and also heating. This system comprises of Sumitomo CH-204SFF cold head, Vacuubrand RZ 14 vacuum pump and Sumitomo HC-4A compressor. In the heating process just temperature controller was used. In this process, temperature was controlled starting from the room temperature to higher temperatures. However, cooling process has more details. In this process, there is two lines to connect the compressor to the cold head. These lines are used for transfer high pressure and low pressure helium gas to cold head and compressor respectively. Cold head has a valve and with the aid of this valve high pressure gas enters the cold head and low pressure gas leaves the cold head and it is transferred into the compressor. Cold head has a sample holder and sample is mounted there. Moreover, cold head has quartz windows which THz radiation is transmitted through and then THz radiation transmitted through the sample. In Figure 2.7 and Figure 2.8 picture of sample holder and cryostat is shown.

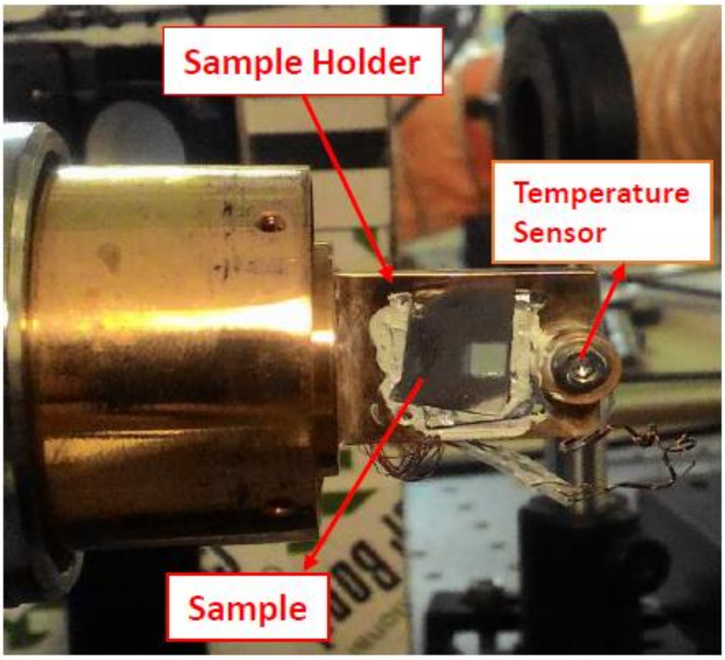

Figure 2.7: Picture of sample holder, sample and temperature sensor.

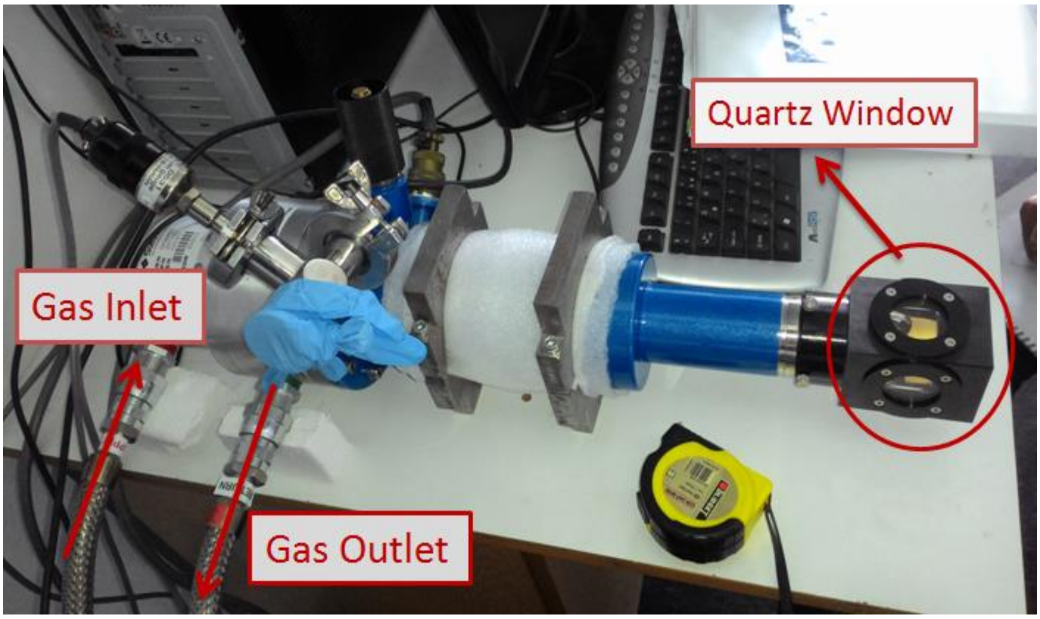

Figure 2.8: Picture of cryostat.

CHAPTER 3

CONDUCTIVITY OF THIN FILMS

Conductivity of thin films can be classified in three categories. Conductivity of metals can be calculated by using classical Drude Model and also superconductor's conductivity is of particular interest since its conductivity at room temperature differ from those at low temperatures such as YBCO. Moreover, conductivity of room temperature insulators which show metallic behavior at high temperatures can be classified in different category such as VO_2.

3.1 Drude Model Conductivity

3.1.1 DC Conductivity

This model was developed by Paul Drude after the discovery of electron by J. J. Thompson [33]. AC and DC conductivity can be calculated by using Ohm's law.

$$V = IR \tag{3.1}$$

where V is the applied voltage, I is the resulting current and R is resistance. Also this formula can be remodeled like

$$\vec{J} = \sigma\vec{E} \tag{3.2}$$

where $\vec{J}$ is the current density, $\vec{E}$ is the applied electric field and σ is conductivity of the metal. According to Drude model assumption, charge carriers have a drift velocity and they move freely in an electric field [34]. Average drift velocity can be expressed as

$$\vec{v} = \mu\vec{E} \tag{3.3}$$

where μ is the carrier mobility and it is given by $\mu = \frac{e\tau}{m}$, here e is the electric charge, m is effective mass of the carriers and τ is relaxation time. Therefore, drift velocity can be written as

$$\vec{v} = \frac{e\tau}{m}\vec{E} \tag{3.4}$$

Moreover, In Eq. 3.2 current density J is defined and it can also be written in that form

$$\vec{J} = ne\vec{v} \tag{3.5}$$

where n is the number of electrons per unit volume. Then, when drift velocity is placed in Eq. 3.5, current density becomes

$$\vec{J} = \frac{ne^2\tau}{m}\ \vec{E} \tag{3.6}$$

Therefore, conductivity of material can be defined as

$$\sigma_{DC} = \frac{ne^2\tau}{m} \tag{3.7}$$

This conductivity called as dc conductivity of material. Applied electric field do not affect the dc conductivity value of the material.

3.1.2 AC Conductivity

Drude model depend on equation of motion of an electron under the electric field [35]. The equation of motion for drift velocity can be expressed as

$$m\frac{d\vec{v}}{dt} + \frac{m\vec{v}}{\tau} = e\vec{E}_0 e^{-i\omega t} \tag{3.8}$$

After applying a sinusoidal electric field, electrons also have a sinusoidal motion and it can be expressed as

$$\vec{v} = \vec{v}_0 e^{-i\omega t} \tag{3.9}$$

Therefore Eq. 3.9 is placed in Eq. 3.8, it can be written as

$$\left(-imv + \frac{m}{\tau}\right)\vec{v}_0 = e\vec{E}_0 \tag{3.10}$$

Thus drift velocity v_0 can be expressed as

$$\vec{v}_0 = \frac{e\vec{E}_0}{(\frac{m}{\tau} - imv)} \tag{3.11}$$

Then, from the Eq. 3.5 it is known that the current density is directly proportional to the drift velocity and carrier density. Therefore, when the Eq. 3.11 is placed into the Eq. 3.5 we have

$$\vec{J} = ne\vec{v}_0 = \frac{ne^2}{\frac{m}{\tau} - imv}\vec{E}_0 \tag{3.12}$$

In addition, from the Eq. 3.2 it is known that current density is directly proportional to conductivity and electric field. Thus complex conductivity can be extracted from the combination of Eq. 3.2 and Eq. 3.12.

$$\sigma = \frac{ne^2\tau}{m}\frac{1}{(1 - i\omega t)} \tag{3.13}$$

Moreover, Eq. 3.13 can be written in the following form by using Eq. 3.7

$$\sigma = \sigma_{DC}\frac{1}{(1 - i\omega t)} \tag{3.14}$$

Therefore, it is frequency dependent complex conductivity. Real and imaginary parts of the ac conductivity can be expressed as

$$\sigma = \sigma_1 + i\sigma_2 \tag{3.15}$$

$$\sigma_1 = \frac{\sigma_{DC}}{1+(\omega\tau)^2} \text{ and } \sigma_2 = \frac{\sigma_{DC}\,\omega\tau}{1+(\omega\tau)^2} \tag{3.16}$$

3.2 Conductivity of Superconductors

H. K. Onnes discovered superconductivity in 1911 after he had liquefied helium in 1908 [36] Therefore he could be able to decrease the temperature to a few degrees of Kelvin. Afterwards, 1950s and also 1960s are very significant dates for emerging acceptable and definite theoretical vision of classical superconductors [37]. Then, in 1986 G. Bednorz and A. Muller discovered high temperature (HT_c) superconductors [36]. HT_c superconductors are quite suitable for THz applications and they also have larger bandgap.

Critical temperature and London penetration depth have significant role for superconductors. Since under the critical temperature, superconductor achieve superconductivity state and it can show characteristics of superconductivity. Quality of superconductors can affect their critical temperature.

In this study, conductivity of superconductors was modeled by using two fluid model. In this model conductivity of superconducting material changes with changing the density of normal and superconducting carriers [38]. Motion of normal carriers and motion of superconducting carriers are controlled by Drude term and London term respectively. Two fluid model is appropriate for under the critical temperature of superconductors. Exponent term, empirical parameter and penetration depth are the examples of characteristic values for superconducting materials and in this study these values were obtained from literature [39], [40].

According to two fluid model, complex conductivity of superconducting film can be expressed as [37]

$$\tilde{\sigma} = \frac{ne^2}{m^*}\left(\frac{f_n(T)}{\frac{1}{\tau}-i\omega} + \frac{if_s(T)}{\omega}\right) \tag{3.17}$$

where f_n is normal carriers fraction and f_s is superconducting carriers fraction, n is the carrier density, m^* is effective mass of carriers and τ is relaxation time. Then when complex conductivity is divided into real and imaginary part we have

$$\sigma_{re} = \frac{ne^2}{m^*}\frac{\tau f_n(T)}{(1+\tau^2\omega^2)} \tag{3.18}$$

$$\sigma_{im} = \frac{ne^2}{m^*}(\frac{f_n(T)\omega\tau^2}{1+\omega^2\tau^2} + \frac{f_s(T)}{\omega}) \tag{3.19}$$

Also it is known that reduced temperature *t* and scattering term is defined by

$$t = \frac{T}{T_c} \tag{3.20}$$

$$\frac{1}{\tau(t)} = \frac{1}{\tau(1)} \frac{t}{1+\alpha(t^{1-\gamma} - t)} \tag{3.21}$$

$$f_s = (1 - \left(\frac{T}{T_c}\right)^{\gamma})^2 \tag{3.22}$$

where γ is exponent term and α is an empirical parameter. Then,

$$f_s(T) + f_n(T) = 1 \tag{3.23}$$

Moreover, plasma frequency is defined by

$$\omega_p = \sqrt{\frac{ne^2}{\varepsilon_0 m^*}} \tag{3.24}$$

Therefore by using this definition real and imaginary conductivity can be expressed as

$$\sigma_{re} = \omega_p^2 \varepsilon_0 \frac{f_n(T)\tau}{(1+\tau^2\omega^2)} \tag{3.25}$$

$$\sigma_{im} = \omega_p^2 \varepsilon_0 \left(\frac{\omega\tau^2 f_n(T)}{(1+\tau^2\omega^2)} \frac{1-f_n(T)}{\omega}\right) \tag{3.26}$$

Therefore by using these formulas conductivity of superconductors can be found and then using Eq. 2.63, values of resistance and reactance can be determined. Afterwards superconducting material can be modeled in CST-Microwave Studio.

3.3 Conductivity of VO_2

Vanadium dioxide shows insulator to metal transition when the temperature is above the critical temperature. Some metal- insulator transitions are due to the electron-electron interaction however in VO_2 it is not the case [41]. Changing the structure of crystal causes a formation of bandgap.

Therefore, insulator to metal transition happened in vanadium dioxide. This phase transition can be actuated thermally electrically and optically [42]. Thus, conductivity of VO_2 depends on temperature, electric field and optical pumping [43] [44]. Bruggeman effective medium theory is used to find conductive properties of $\mathrm{VO_2}$.

Firstly to find the dielectric function of $\mathrm{VO_2}$ in the metallic state simple Drude form is followed [45]

$$\varepsilon_m(w) = \varepsilon_\infty - \frac{\omega_p^2}{i\gamma\omega+\omega^2} \tag{3.27}$$

where ε_∞ is high frequency dielectric function, w is cyclic frequency, w_p is plasma frequency and γ is damping constant. Plasma frequency is defined in Eq. 3.24. Cyclic frequency and damping constant can be written in the following forms

$$\omega = 2\pi v \tag{3.28}$$

$$\gamma = \frac{e}{m^*\mu} \tag{3.29}$$

where μ s mobility of charge carriers. Also effective mass of the charge carriers can be expressed as $m^* = 2m_e$ and here m_e is mass of the electron.

Boltzmann function can be used for the modulation of the temperature [32] [46]

$$f(T) = f_{max}\left[1 - \frac{1}{1+e^{\left(\frac{T-T_0}{\Delta T}\right)}}\right] \tag{3.30}$$

where f is the volume fraction of metallic domain and f_{max} is volume fraction at highest temperature for metallic phase, ΔT is hysteresis temperature and this value is taken from literature [45] [46]. In addition, T_0 is transition temperature.

Therefore, effective dielectric function of $\mathrm{VO_2}$ from the Bruggeman effective medium theory can be expressed as

$$\varepsilon_{eff} = \frac{1}{4}\{3f(\varepsilon_m - \varepsilon_i) + 2\varepsilon_i - \varepsilon_m \mp \sqrt{(3f(\varepsilon_m - \varepsilon_i) + 2\varepsilon_i - \varepsilon_m)^2 + 8\varepsilon_i\varepsilon_m}\} \quad (3.31)$$

where ε_m and ε_i are dielectric functions of metallic and insulating domain, respectively. ε_m is expressed in Eq. 3.27. Moreover, from the previous research [45] [47], high frequency dielectric function ε_∞ , insulating domain dielectric function ε_i, carrier density n and carrier mobility can be determined.

Relation between dielectric function and conductivity is expressed as

$$\sigma_{eff} = -i\omega\varepsilon_0(\varepsilon_{eff} - 1) \quad (3.32)$$

CHAPTER 4

EXPERIMENTAL RESULTS

In this thesis, different shape of metasurface structures and different substrates were used to investigate the conductive properties of thin films. These thin films were characterized by using THz-TDS system. Studies were done for unpatterned YBCO and VO_2. Also, quadcross shape patterned gold, YBCO and cross shape patterned VO_2 on dielectric substrates such as sapphire and fused silica were characterized. Shapes of these structures can be seen in Fig. 4.1. These samples were fabricated in Izmir Institute of Technology (IZTECH).

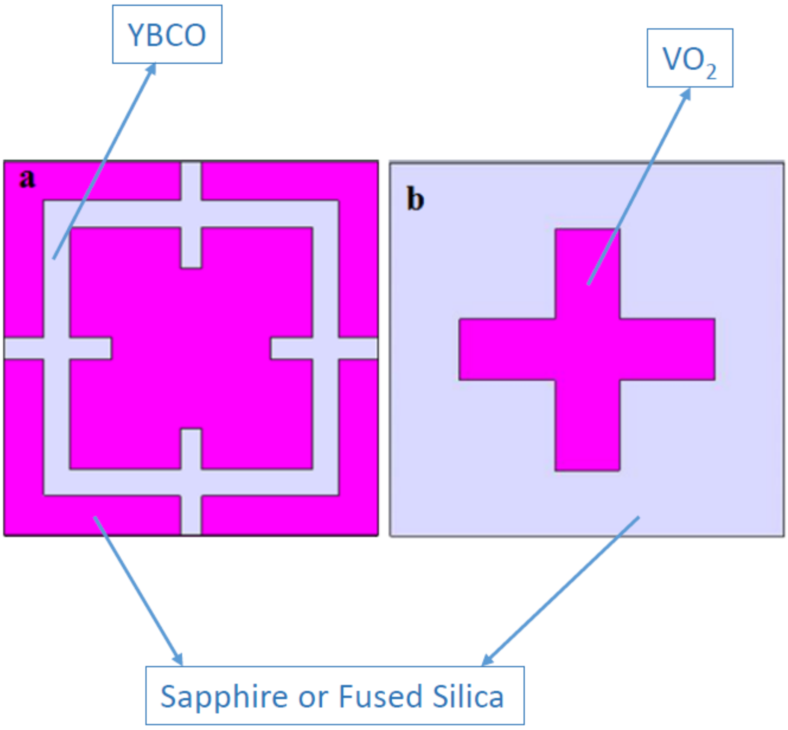

Figure 4.1: a) Qaudcross shape structure b) Cross shape structure.

4.1 Single Layer YBCO on Top of Fused Silica Substrate

In this part, 80 nm thick single layer YBCO film on fused silica substrate were measured by using THz-TDS system. These measurements were done for 20K, 40K, 60K, 65K, 70K, 75K, 80K, 85K, 90K, 95K, 100K, 120K and 298K. Electric field amplitude of the transmitted wave varies significantly when the temperature is decreased. Since under the critical temperature YBCO sample is in the metallic state and it reflects THz radiation. When the sample becomes metallic, its conductivity will increase.

In Figure 4.2 changes in the THz electric field amplitude at different temperatures can be seen.

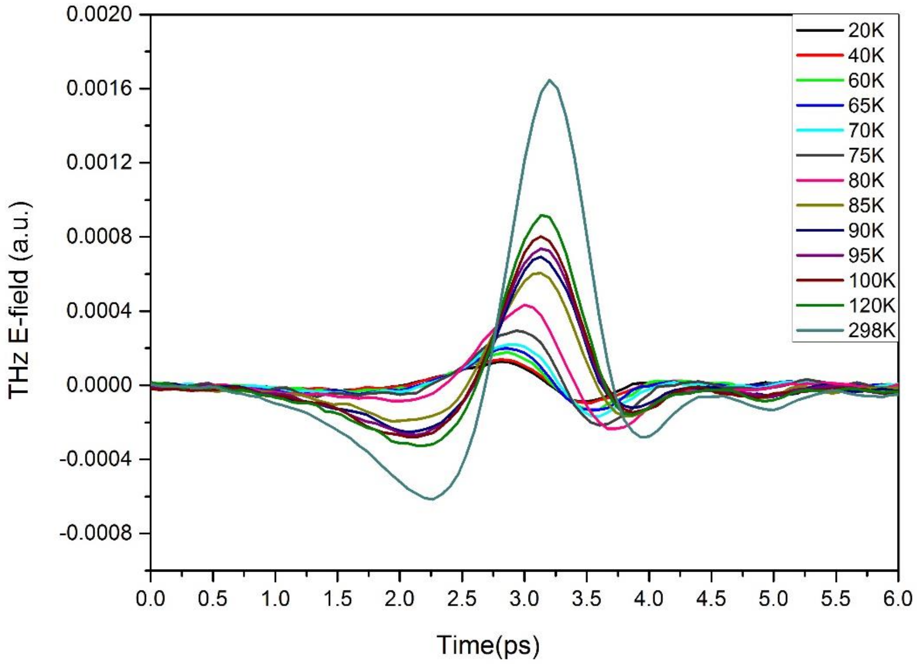

Figure 4.2: THz E-field in time domain at different temperatures for single layer YBCO.

In Figure 4.3 and Figure 4.4 frequency dependent results of real and imaginary part of the conductivity at different temperatures is shown, respectively. These results are found by using Eq. 3.25 and Eq. 3.26 in Chapter 3 by using two fluid model.

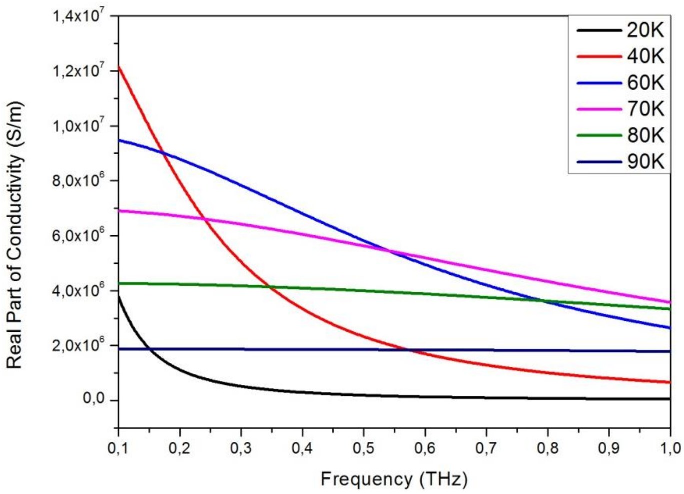

Figure 4.3: Simulation result for real part of conductivity for 80 nm thick YBCO with respect to frequency.

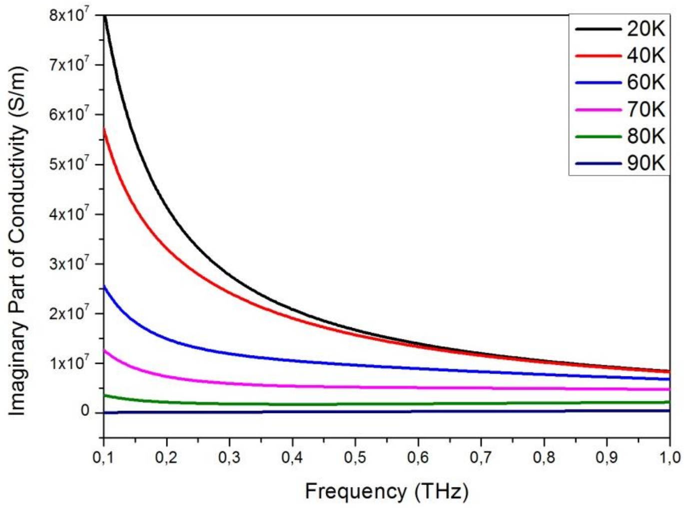

Figure 4.4: Simulation result for imaginary part of conductivity for 80 nm thick YBCO film with respect to frequency.

In Figure 4.3, it can be seen that when frequency is decreased real part of conductivity at several temperatures increases. Also in low temperatures real part of conductivity depend on frequency more than high temperatures. Moreover, real part of the conductivity started to increase by decreasing the temperature from 90K to 70K. After that, real part of the conductivity started to decrease. In addition, when imaginary part of the conductivity is considered in two fluid model it is expected to dependence of frequency follows $1/\omega$ function. In Figure 4.4, when temperature is decreased imaginary part of the conductivity increases. These results of conductivities was used to calculate transmission structure of YBCO film.

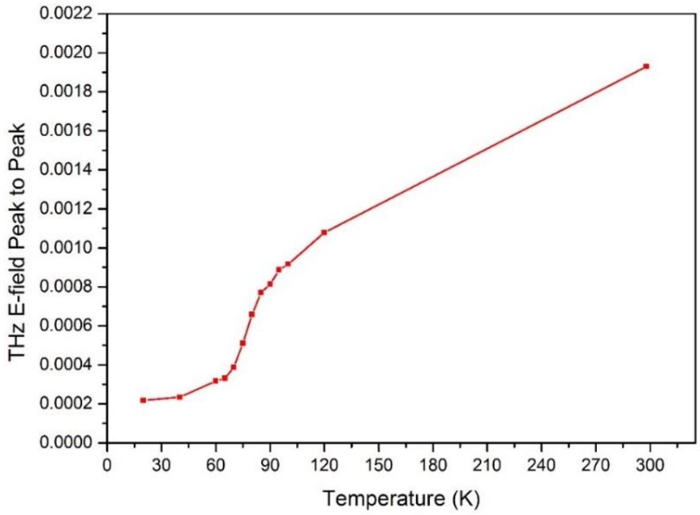

Figure 4.5: THz E-field peak to peak values for 80 nm thick single layer YBCO at different temperatures.

Also, in Figure 4.5, by using peak to peak values of THz E-field at different temperatures it can be said that critical temperature of single layer YBCO is near 90K.

4.2 Quadcross Shape Patterned YBCO on Top of Sapphire Substrate

In this part quadcross shape patterned 80 nm thick YBCO film on sapphire substrate was investigated by using THz-TDS system. In this measurement closed cycle cryostat was used to control the temperature. Moreover, dimensions, front and side view of the quadcross YBCO can be seen in Figure 4.6 and Figure 4.7. Samples were fabricated at IZTECH. Measurements were done at different temperatures such as 20K, 40K, 60K, 70K, 80K, 84K, 86K, 90K and 100K. CST-Microwave Studio is used to find the simulation result of quadcross YBCO on top of sapphire substrate. In order to determine the surface impedance values formulas for superconductor's conductivity in Chapter 3 is used.

ε_0 (F/m)	μ_0 (H/m)	ω_p (1/s)	γ (1/s)
$8{,}854 * 10^{-12}$	$1{,}256 * 10^{-6}$	$2434 * 10^{12}$	1,9
T_c (K)	d (m)	Z_0 (Ω)	τ_1
90	$80 * 10^{-9}$	377	$3{,}57 * 10^{-14}$

Table 4.1: Simulation parameters for finding conductivity of YBCO film.

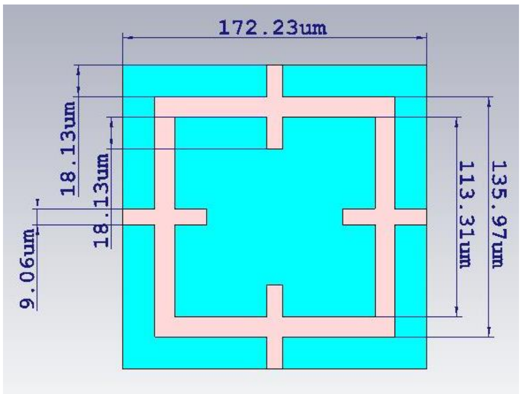

Figure 4.6: Front view and dimensions of the quadcross YBCO film on sapphire substrate.

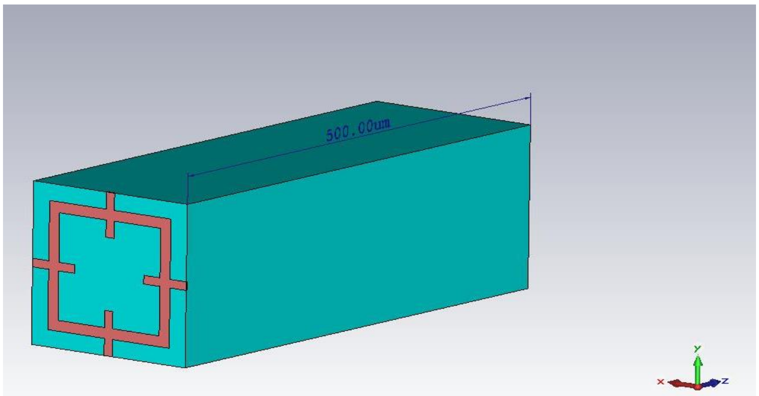

Figure 4.7: Side view of quadcross YBCO film on of 500 μm thick sapphire substrate.

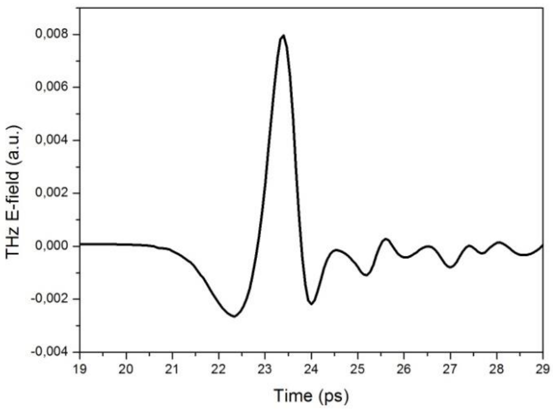

Figure 4.8: THz E-field vs. frequency graph for 500 micrometer thick sapphire substrate.

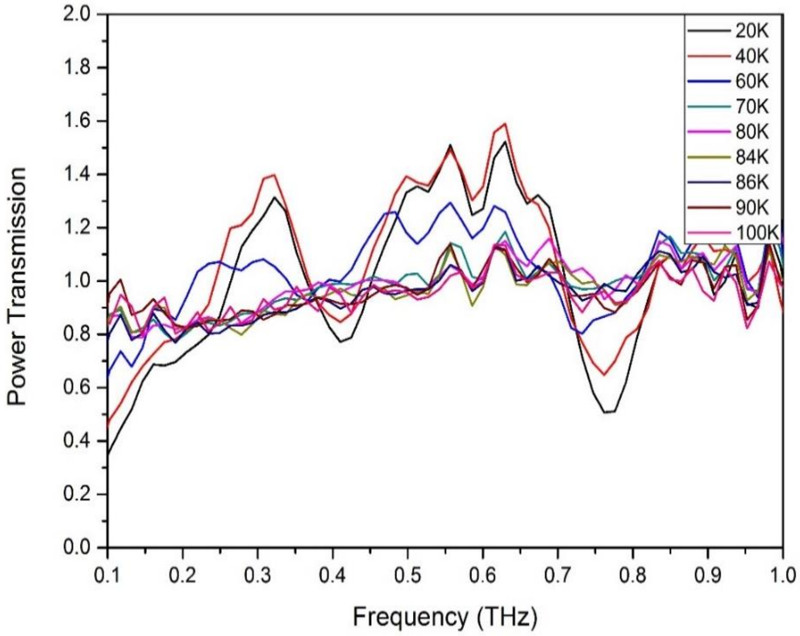

Figure 4.9: Experimental power transmission result for quadcross YBCO film on sapphire substrate.

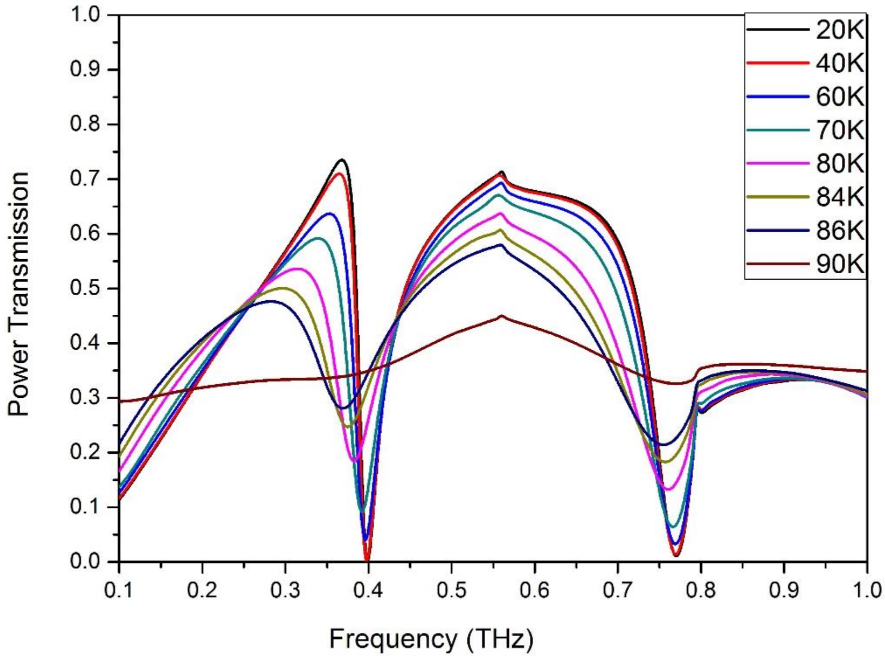

Figure 4.10: Simulation power transmission result for quadcross YBCO film on sapphire substrate.

In Figure 4.9 and Figure 4.10 experimental and simulation results of power transmission for quadcross YBCO can be seen. Conductivity of YBCO is changed when the temperature is changed. Therefore, there are different power transmission results for each temperature. When simulation and experimental results were compared it can be seen that resonance frequencies are in agreement with each other. In Figure 4.9 power transmission at 298K is referenced to the transmission at different temperatures. When the experimental power transmission is compared to the simulation result of the power transmission, they are different from each other. Since simulation were performed by using data from literature [39] [40]. Resonance frequencies of quadcross patterned YBCO film is shifted when temperature is changed. For example, when the temperature is 20K, it shows resonance both 0.411 THz and 0.766 THz. However when the temperature is increased to 40K, resonance frequency is shifted to 0.410 THz and 0.761 THz.

4.3 Quadcross Shape Patterned Gold on Top of Fused Silica Substrate

In this part quadcross shape patterned 130 nm thick gold film on top of fused silica substrate was investigated by using THz-TDS system. Dimensions and structure are same as quadcross YBCO and it can be seen in Figure 4.6 and Figure 4.7. Although temperature was changed, resonance shift and modulation were not observed. Since conductivity of YBCO film changed with temperature change. However, conductivity of gold film do not depend on temperature change and so temperature change do not effect conductivity of gold film. Therefore, resonance frequency of quadcross gold film is same in all temperature. Experimental and simulation results of quadcross gold film can be seen in Figure 4.11 and Figure 4.12. For this simulation parameters for Gold film is shown in Table.

Electrical conductivity (S/m)	$\boldsymbol{\mu}$
$4{,}561 * 10^7$	1

Table 4.2: Simulation parameter for quadcross shape patterned gold in CST-MW Studio.

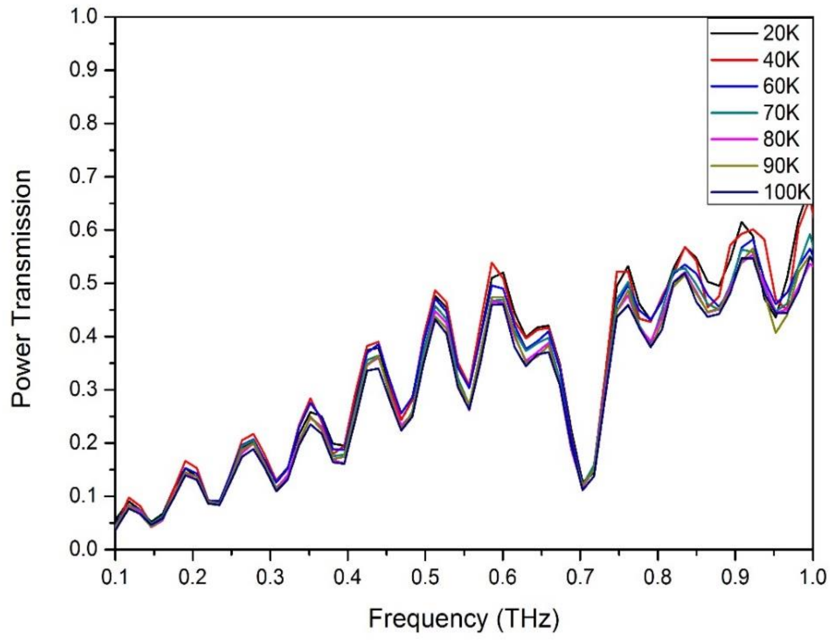

Figure 4.11: Experimental power transmission result for quadcross gold film on fused silica substrate.

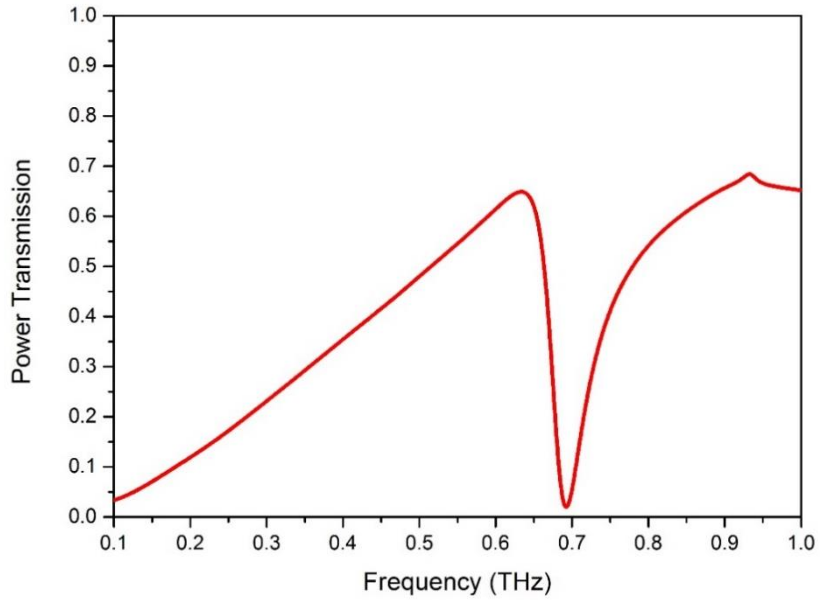

Figure 4.12: Simulation result of power transmission for quadcross gold on fused silica substrate.

4.4 Unpatterned VO_2 on Top of Sapphire Substrate

In this part, 250 nm thick unpatterned VO_2 on top of sapphire substrate was investigated by using THz-TDS system. Measurements were done at different temperatures such as 291K, 310K, 330K, 340K, 350K, 360K and 370K. In these measurements closed cycle cryostat is used only in heating mode. Therefore measurements started from room temperature. These films were fabricated in IZTECH and by using dc magnetron sputtering VO_2 films were coated on c-cut sapphire and fused silica substrates. Same conditions were used for growing these films on both fused silica and sapphire substrate. After substrates were ultrasonically cleaned and dried, they were placed into the vacuum chamber. Contaminations on the surface of V target were took away by pre-sputtering. DC power was utilized to V target. Temperature of substrate is increased and it was kept constant at 550 ^{o}C during the deposition process. Moreover, film surface homogeneity was improved by rotating at 15 rpm.

In Figure 4.13 it can be seen that electric field amplitude of the transmitted wave alters significantly. Moreover, in Figure 4.14 power transmission with respect to frequency is obtained by applying Fourier transform on time dependent waveforms. Critical temperature of VO_2 is nearly in 340K. Jepsen *et al*. also found in previous works that critical temperature of VO_2 is 68 ^{o}C. This result is in agreement with previous works. Therefore below the critical temperature VO_2 film is transparent for THz radiation and above the critical temperature VO_2 film reflects THz radiation. Thus, above the critical temperature VO_2 film is in the metallic state and below the critical temperature it is in insulating state.

ε_0 (F/m)	μ_0 (H/m)	ω_p (1/s)	γ (1/s)	μ (m^2/V.s)
$8,854 * 10^{-12}$	$1,256 * 10^{-6}$	$4,5477 * 10^{15}$	$4,3963 * 10^{14}$	$2 * 10^{-4}$
N (m^{-3})	e (C)	ΔT (K)	d (m)	ε_i , ε_∞
$1,3 * 10^{28}$	$1,602 * 10^{-19}$	4	$250 * 10^{-9}$	9

Table 4.3: Parameters for finding conductivity model of VO_2 film.

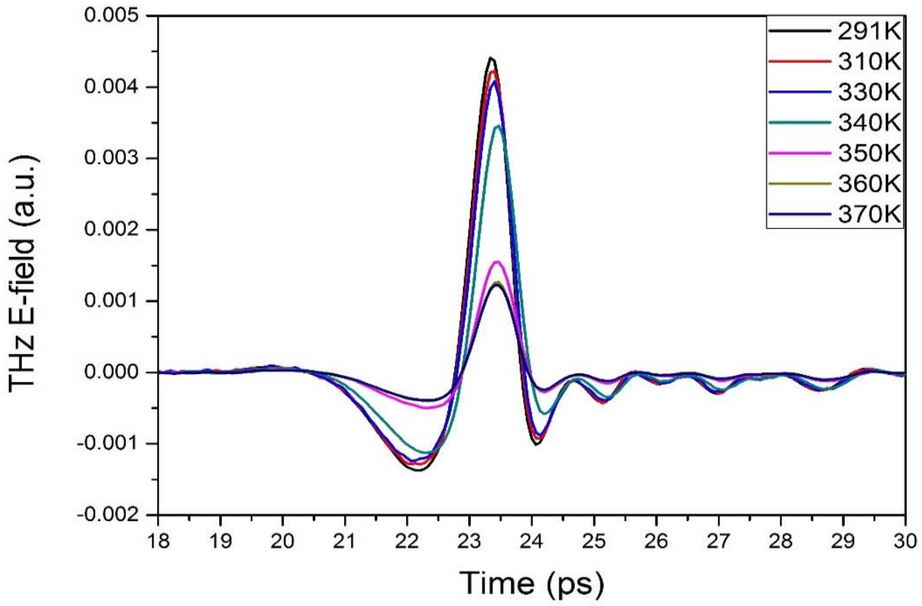

Figure 4.13: THz E-field in time domain at different temperatures for unpatterned VO_2 on sapphire substrate.

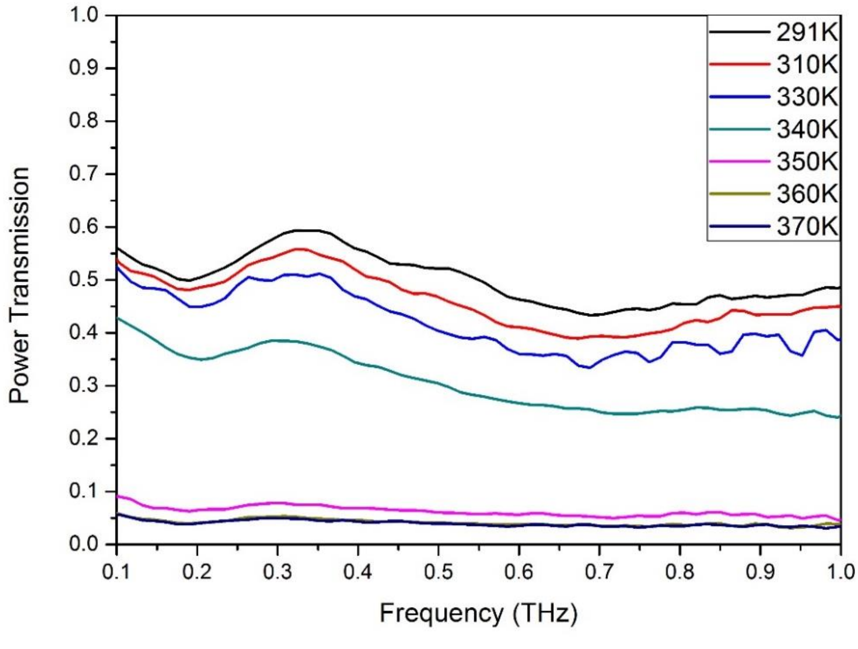

Figure 4.14: Experimental power transmission result for unpatterned VO_2 on sapphire substrate.

In order to find simulation result of power transmission for unpatterned VO_2 on sapphire substrate, conductivity was found by using Bruggeman effective medium theory given in Chapter 3. However, simulations of VO_2 film cannot be done with CST-Microwave Studio 2015. Therefore, by using methods in Chapter 3 and Chapter 2, it is tired to derive by ourselves.

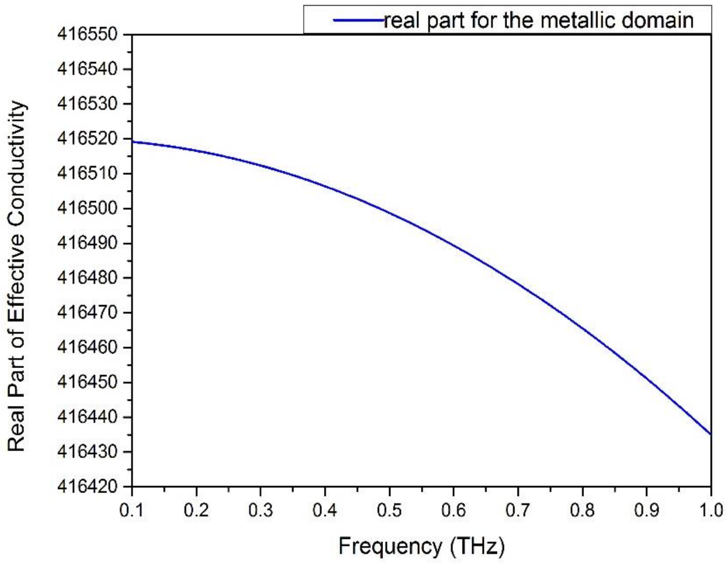

Figure 4.15: Real part of the effective conductivity for the metallic domain vs. frequency.

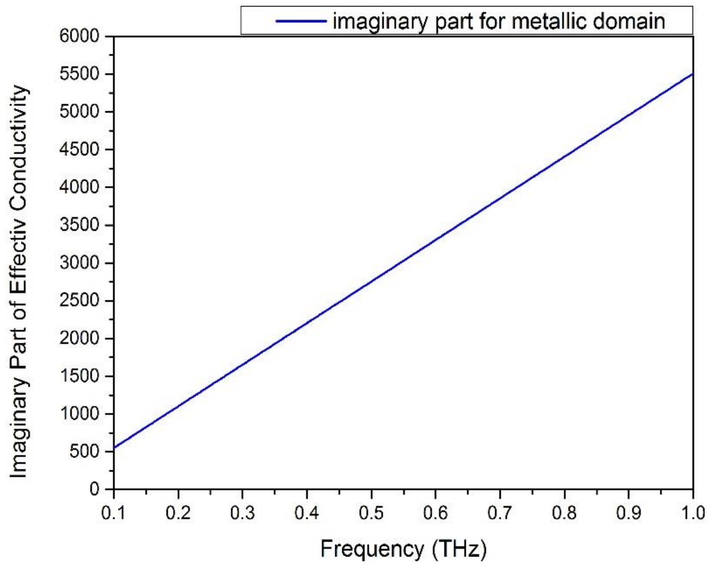

Figure 4.16: Imaginary part of the effective conductivity for the metallic domain vs. frequency.

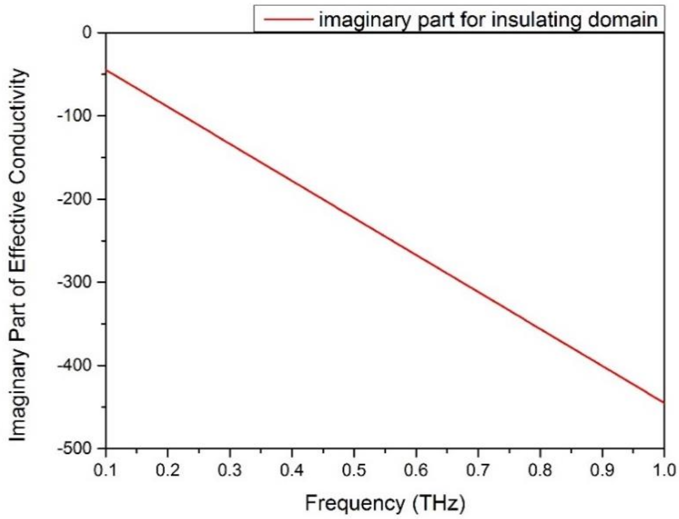

Figure 4.17: Imaginary part of the effective conductivity for insulating domain vs. frequency.

In Figure 4.15 and Figure 4.16 real and imaginary part of effective conductivity is shown for metallic domain. According to phase transition of VO_2, sample is in the metallic state when the temperature is above the critical temperature. Therefore, above 340 K, sample is in the metallic state. Also, imaginary and real part of conductivity for this sample at 340 K, 350 K, 360 K and 370 K should change like Figure 4.15 and Figure 4.16 according to theoretical model in Chapter 3. Experimental results for conductivity measurement is also shown in Figure 4.18 and Figure 4.19 according to Chapter 2. In the experimental results, imaginary part of conductivity in the metallic domain is increased and it can be said experimental and theoretical results are almost in agreement with each other for metallic domain. However, real part of the conductivity results in metallic domain are not in agreement with each other. Moreover, VO_2 film is in the insulating state at 330 K, 310 K and 291 K. Therefore, there should be only imaginary part of conductivity for these temperatures according to theoretical model in Chapter 2. However, in experimental result there is also real part at these temperatures. According to theoretical results for imaginary part in Figure 4.17, in insulating domain imaginary part of conductivity should be below zero. In experimental results in Figure 4.19, at 330 K, 310 K and 291 K nearly 0.5 THz conductivity below zero. However, after 0.5 THz it starts to increase and it is unexpected result for insulating domain.

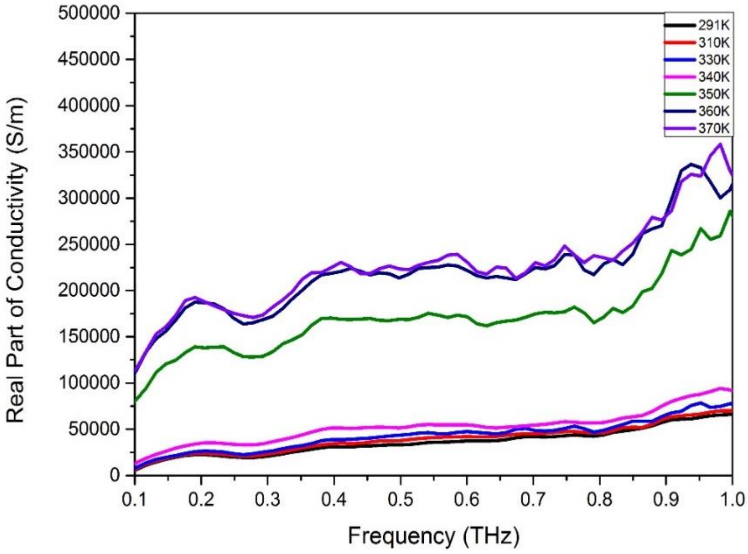

Figure 4.18: Real part of the conductivity of VO_2 which is calculated by using method in Chapter 2.

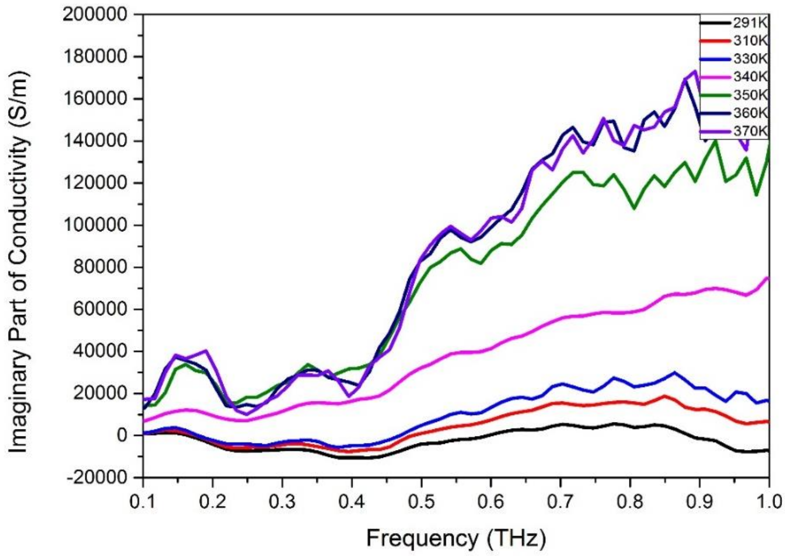

Figure 4.19: Imaginary part of the conductivity of VO_2 which is calculated by using method in Chapter 2.

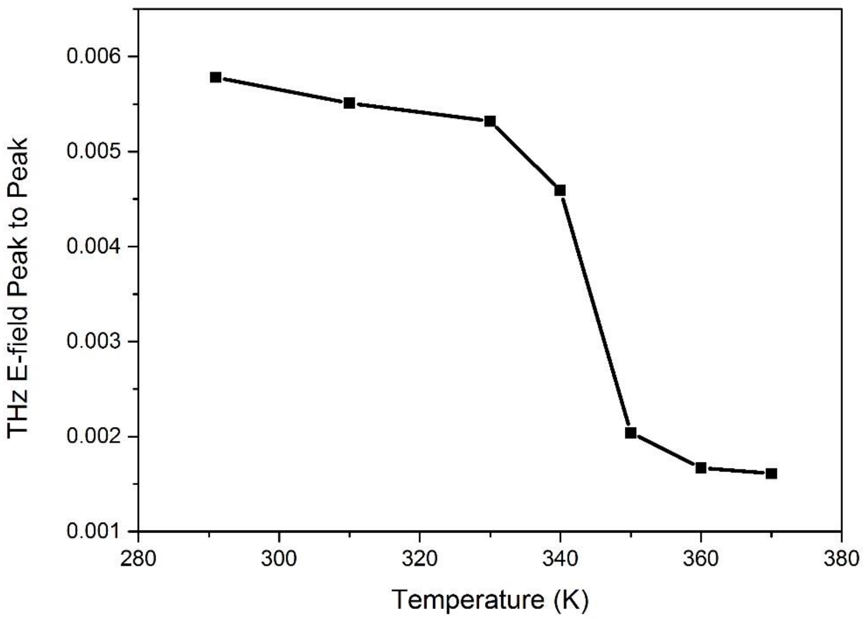

Figure 4.20: THz E-field peak to peak values for unpatterned VO_2 on top of sapphire substrate.

4.5 Cross Shape Patterned VO_2 on Top of Sapphire Substrate

In this part, cross shape [48] patterned 250 nm thick VO_2 on 500 μm sapphire substrate was investigated. Measurements were done at 299K, 310K, 330K, 340K, 350K, 360K and 370K. Dimensions, side view and front view of cross shape patterned structure is given in Figure 4.21 and Figure 4.22. Moreover, in Figure 4.23 there is optical microscope image and photograph of this structure. In addition, Figure 4.25 shows difference in E-field amplitude at different temperatures. In Figure 4.26 in power transmission graph only etalon effect is observed. Also, In Figure 4.27 experimental result of power transmission for cross shaped patterned VO_2 by eliminating etalon effect is given. In this graph power transmission at 299K or room temperature is normalized to higher temperatures. Therefore, this ratio is expected to be greater than 1.

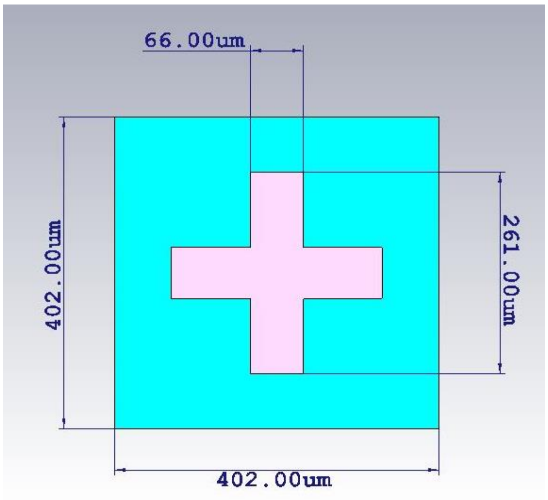

Figure 4.21: Front view and dimensions of cross shape patterned VO_2 on top of sapphire substrate.

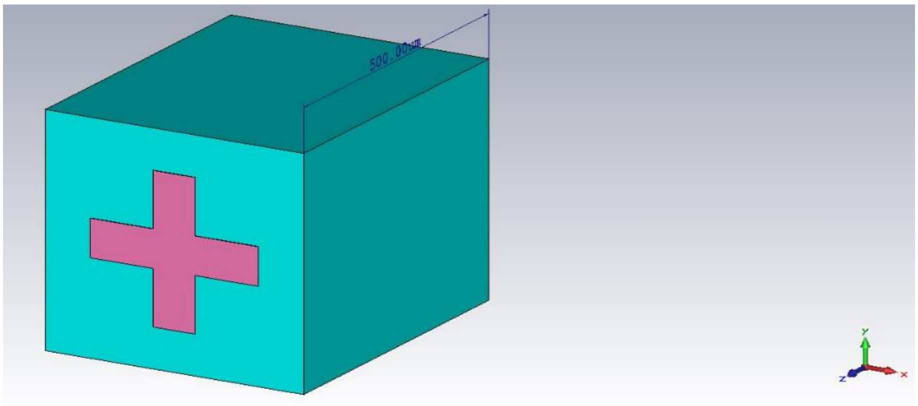

Figure 4.22: Side view of VO_2 on top of 500 µm sapphire substrate.

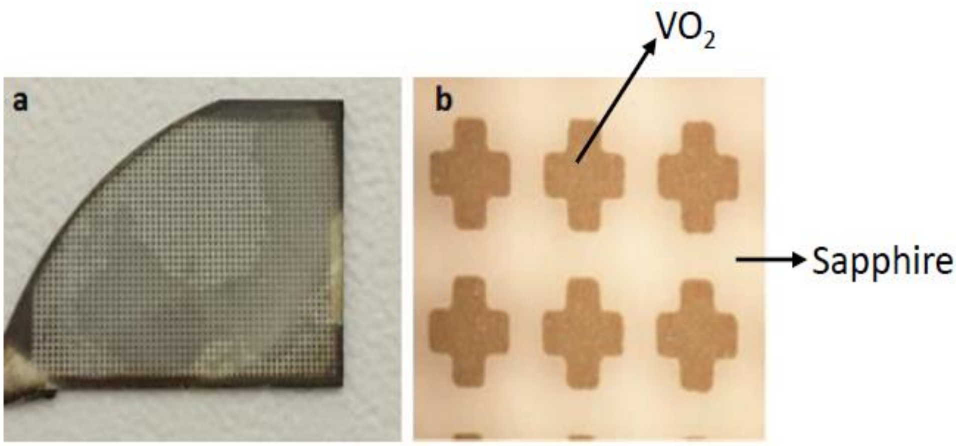

Figure 4.23: a) Photograph and b) microscope image of VO_2 on top of sapphire substrate.

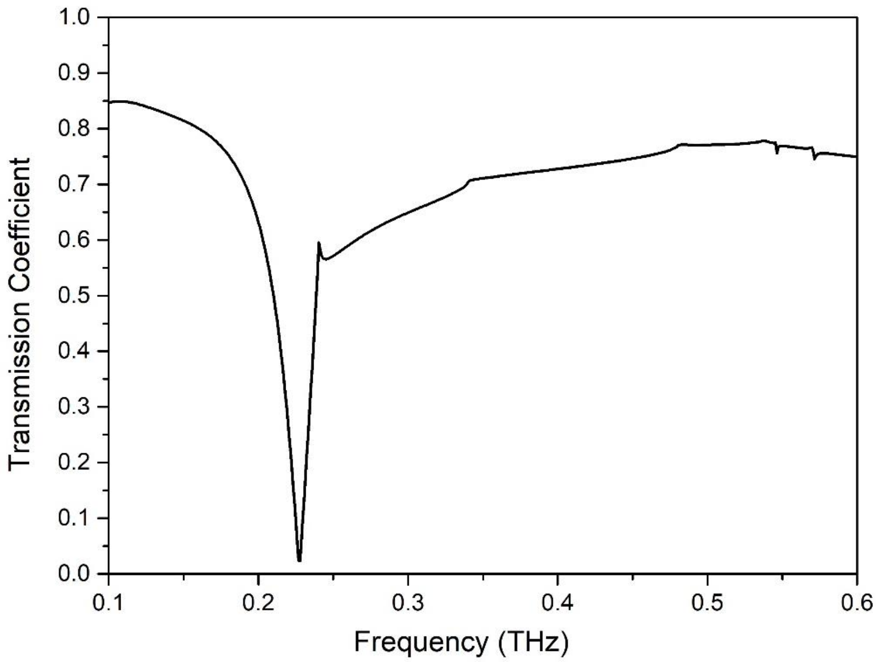

Figure 4.24: Transmission coefficient vs. frequency graph of gold on sapphire substrate with the same dimension of cross shape structure.

In Figure 4.24, simulation result of cross shape gold on top of 500 μm sapphire substrate is given. In this simulations structure and dimensions are same with Figure 4.21 and Figure 4.22. However, instead of using VO_2 film, gold film is used to find the transmission properties of high conductive sample. In this Figure, since film is gold and it is high conductive in contrast with VO_2 film, resonance frequency is clearly seen. Also, differences in transmission coefficient can be seen in the next pages between high and low conductive samples in Figure 4.31 and Figure 4.32.

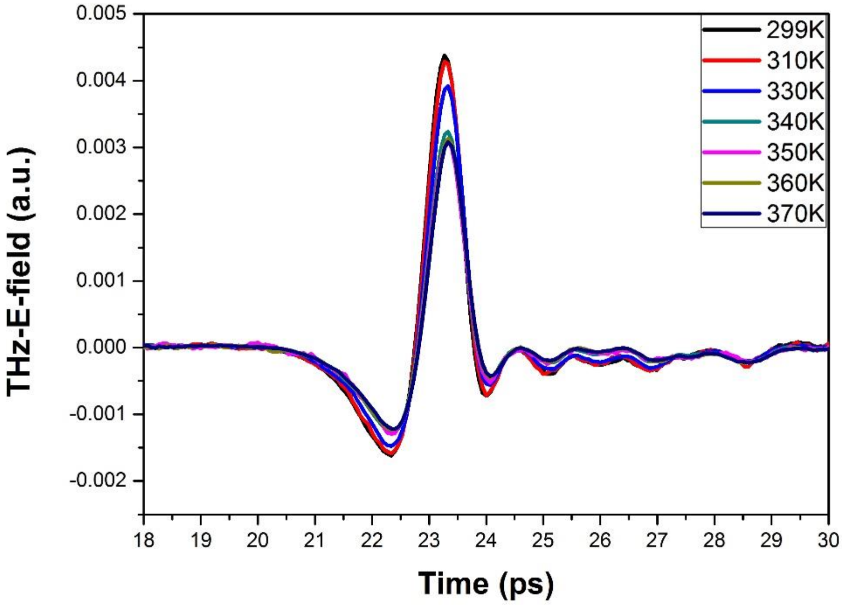

Figure 4.25: THz E-field in time domain at different temperatures for cross shape patterned VO_2 on top of sapphire substrate.

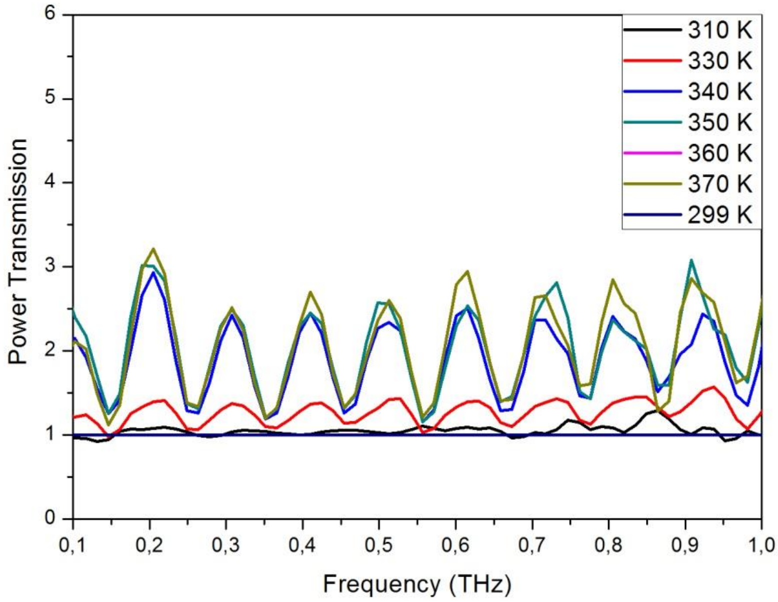

Figure 4.26: Experimental power transmission result for cross shape patterned VO_2 on top of sapphire substrate. The transmission at 299K is normalized to those of higher temperatures.

In Figure 4.26 etalon effect was observed and it became more clear with increasing the temperature. Also this effect can be analysed to understand refractive index or thickness of the substrate. Therefore refractive index of sapphire substrate can be found by using ;

$$\Delta f = \frac{c}{2nd} \tag{4.1}$$

where c is the speed of light in mm and thickness of sapphire substrate is d also it is in mm.

Figure 4.26 was used to find peak difference of the frequency and it is equal to 0.103 THz. At different temperatures real refractive index of sapphire was calculated at different temperatures and it can be seen in Table 4.4. According to measurement refractive index of sapphire substrate was not change when temperature is changed and it is 2.93 according to calculations. Moreover, according to previous measurement it is nearly 3.00 [1].

Temperature (K)	310	330	340	350	360	370
Refractive index	2.93	2.93	2.93	2.93	2.93	2.93

Table 4.4: Refractive index of sapphire substrate according to temperature.

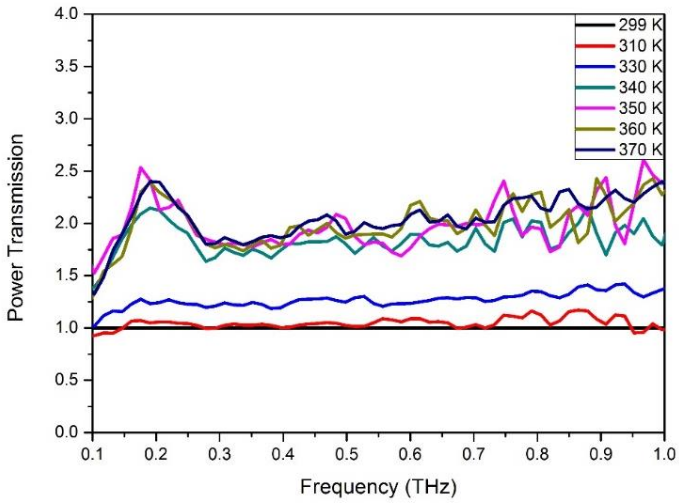

Figure 4.27: Experimental power transmission result for cross shape patterned VO_2 on top of sapphire substrate by eliminating etalon effect.

4.6 Cross Shape Patterned VO_2 on Top of Fused Silica Substrate

In this part dimensions and structure are same as previous part. However, thickness of fused silica substrate is 900 μm. Measurements are also done in same temperatures. In Figure 4.28 there is an image and microscope image of this film.

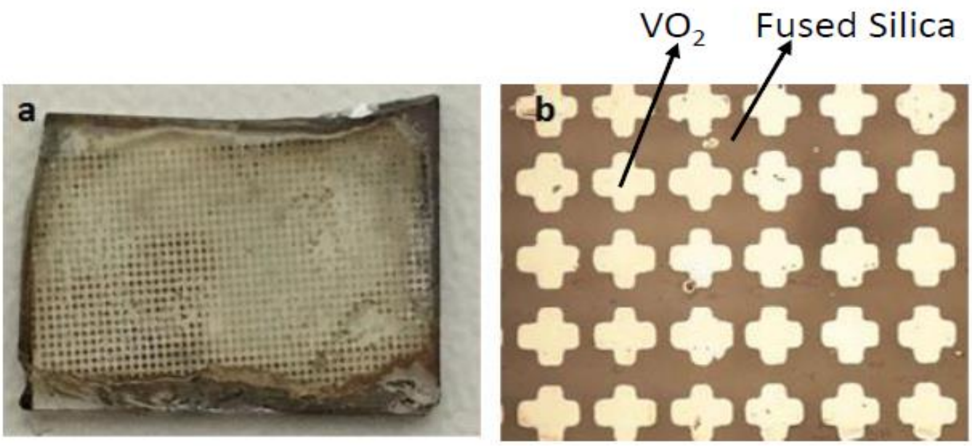

Figure 4.28: a) Photograph and b) optical microscope image of VO_2 on top of 900 μm thick fused silica substrate.

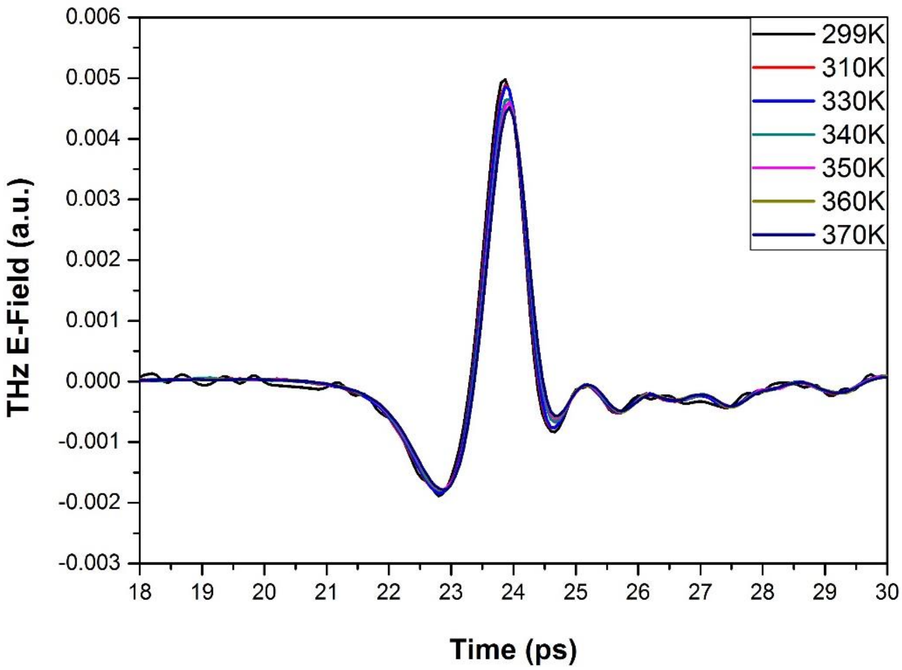

Figure 4.29: THz E-field in time domain at different temperatures for cross shape patterned VO_2 on top of fused silica substrate.

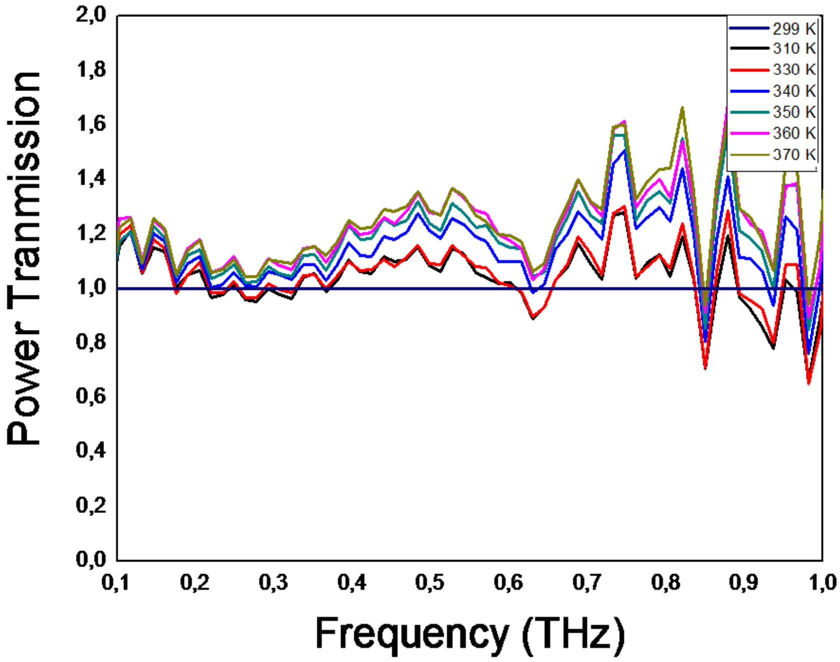

Figure 4.30: Experimental power transmission result for cross shape patterned VO_2 on top of fused silica substrate.

In Figure 4.29 electric field amplitude of this structure can be seen at different temperatures. Moreover, in Figure 4.30 power transmission at different temperatures are given in frequency domain. Again power transmission is normalized to the higher temperatures so ratio is greater than 1. In cross shape pattern on top of sapphire substrate etalon effect is tried to eliminate and here etalon effect are not apparent. Interference is required in order to see etalon effect. However, in sapphire substrate interference is greater than fused silica substrate. Therefore, in fused silica substrate etalon effect cannot be seen. Moreover, refractive index of sapphire and fused silica are different from each other. According to previous researches refractive index of sapphire substrate is nearly 3 and fused silica is nearly 2 [1]. When power reflections from one interface are compared, it is approximately %25 in sapphire and in fused silica it is approximately %11. This is the other reason why etalon effect cannot be seen in fused silica substrate.

In this cross shape patterned VO_2 on sapphire and fused silica substrate it is expected to see effect of bandpass filtering and frequency selective properties of patterned VO_2. However, due to the small change in conductivity between insulator and metallic states it was not observed as was expected. For example, in Figure 4.31 transmission coefficient vs. frequency graph of high conductive sample is shown. In addition to this in Figure 4.32 it is possible to show behavior of the sample which have low conductivity. Therefore effect of bandpass filtering cannot observed in patterned VO_2 film. This simulations are for positive cross on negative substrate.

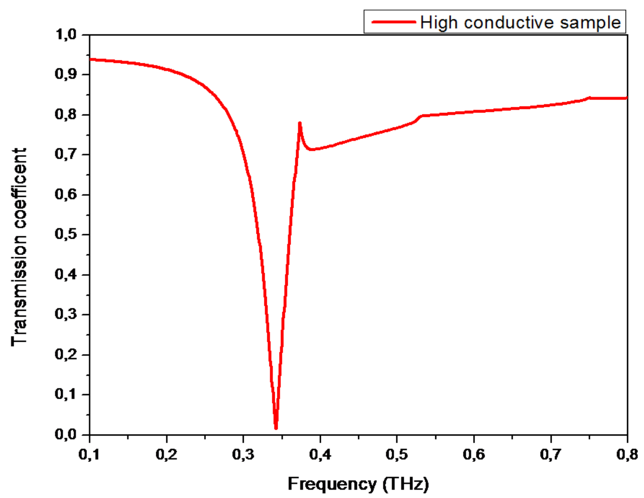

Figure 4.31: Transmission coefficient vs. frequency graph for high conductive sample.

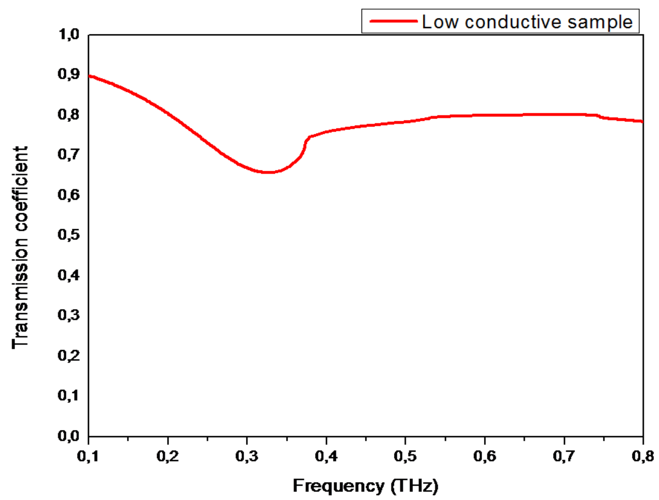

Figure 4.32: Transmission coefficient vs. frequency graph for low conductive sample.

In this results high conductive sample is considered as Gold and its conductivity parameter are same as Table 4.2 and by using this parameter simulation results are obtained for high conductive sample. Moreover, for low conductive sample in order to define this material surface impedance table is used in CST and these parameters can be shown in Table 4.5.

Frequency (THz)	**Resistance (Ohm/sq)**	**Reactance (Ohm/Sq)**
0.1	70	0
1	70	0

Table 4.5: Parameters for finding effect of bandpass filtering in low conductive sample.

CHAPTER 5

CONCLUSION

In this study, different thin films such as gold, YBCO and VO_2 and different structures of them such as quadcross and cross shapes were characterized and their conductive properties on different substrates were investigated. In these measurements THz-TDS system is used. Moreover, these measurements took place at different temperatures. Therefore, to change and control the temperature closed cycle cryostat was used. Also samples were mounted on sample holder of cryostat's cold head as expressed in Chapter 2. In some measurement for example in the measurement of YBCO and gold thin films, cryostat is used for the purpose of cooling because in low temperatures such as below the critical temperature YBCO film behaves as metal. Cryostat also used in the heating mode only because VO_2 film changes its phase in higher temperatures such as above the critical temperature it shows metallic behavior.

In this study, firstly 80 nm thick single layer YBCO film on top of fused silica substrate is investigated by using THz-TDS system. YBCO is a superconductor. In figures at Chapter 4, it is clear that, when temperature is decreased amplitude of THz electric field also decreases. Then it is obvious that when the temperature is decreased level of transmission also decreases. For example, high level of transmission occurs at 298 K and transmission of THz radiation is in the lower state when the temperature is 20K. Since under the critical temperature YBCO film shows metallic behavior and it reflects THz radiation. Thus, when temperature is decreased, conductivity of YBCO film increases. Therefore, at low temperatures YBCO film has high conductivity and at high temperatures conductivity of YBCO film has low conductivity. Also critical temperature of YBCO film is approximately 90K. After examining the critical temperature of single layer YBCO film and behavior this film above and below the critical temperature, quadcross shape patterned 80 nm thick YBCO film on sapphire substrate was investigated by using THz-TDS system at different temperatures. Experimental and simulation result of power transmission were given in Chapter 4. When experimental result is considered, resonance frequencies were both 0.411 THz and 0.766 THz at 20K. Then at 40K resonance frequencies have different values than 20K and these frequencies were 0.410 THz and 0.761. Therefore according to figures which shown in Chapter 4, it is clear that at different temperatures, different resonance frequencies and different power transmission amplitude was observed. Moreover, in order to determine the complex conductivity of YBCO film, formulas in Chapter 3 about conductivity of superconductors is used. In this calculation, some parameters such as plasma frequency were used from the literature [40]. After conductivity of YBCO film was found, simulation result of quadcross patterned YBCO film was obtained by using CST-MW Studio. When simulation result of quadcross patterned YBCO film was considered, resonance frequencies at 20K and 40K are in agreement with each other. However, in simulation results it also showed resonance in different temperatures from 20K to 86K. Moreover, when simulation and experimental results of power transmission is compared, results are different from each other. It is because in simulation some parameters were taken from literature [39], [40]. For example, these parameters are plasma frequency, penetration depth and scattering time. Therefore, there are some differences between simulation and experimental result for quadcross shape patterned YBCO film.

In addition to quadcross YBCO film on top of sapphire substrate, with the same dimensions and quadcross shape Gold film was investigated. These measurements also took place at different temperatures. Unlike superconductors, temperature variation did not affect the conductivity of gold film. Therefore, resonance frequency of quadcross patterned gold film did not change at different temperatures. Experimental and simulation results are in agreement with each other. However, in experimental result of power transmission, etalon effect can be seen due to the thickness of substrate and quartz windows on the cold head.

Furthermore, unpatterned 250 nm thick VO_2 on sapphire substrate is used to find the conductive properties of this film in THz frequency range. According to measurement critical temperature of VO_2 was found at nearly 340K. Below the critical temperature VO_2 was in insulating state and in this state it was transparent to the THz radiation.

However, above the critical temperature VO_2 film was in the metallic state and it blocked incoming THz radiation. Then it is obvious that when temperature is increased, level of transmission of THz radiation decreases. In this case high level of transmission occurs at 291K and transmission of THz radiation is in the lower state when temperature is 370K. Therefore, conductivity of VO_2 film increases when the temperature is increased. Then below the critical temperature its conductivity decreases since the film is in the insulating state. Simulations of unpatterned VO_2 film cannot be done with CST-MW Studio 2015. According to CST workers newer versions of CST program can handle it. However, by using different methods which is given in Chapter 3 Bruggeman effective medium theory and in Chapter 2 calculation of sheet conductivity, it is tried to be done without using CST program. Therefore two models are used to find conductive properties of VO_2 film. According to comparison between experimental and theoretical models of conductivity for VO_2 film, they are not in agreement with each other. In Chapter 2, experimental model of conductivity is not suitable for VO_2 film. It might be suitable for multilayer graphene. After investigating the critical temperature and transmission properties of VO_2 film on top of sapphire substrate, cross shape patterned VO_2 on top of 500 μm sapphire and 900 μm fused silica substrate were investigated by using THz-TDS system. In these samples frequency selective nature of cross shape patterned VO_2 was not obtained as was expected because in between the metallic and insulating state conductivity of VO_2 change is small. Moreover, differences in refractive index of sapphire and fused silica cause different results of power transmission.

There are several applications of THz technology for the purpose of imaging, communication and spectroscopy. One of the most important applications of THz technology is development of THz-TDS system. Characterization of dielectrics, semiconductors and superconductors are made by scientist by using this system. Conductivity of some smart materials changes by switching some parameters such as temperature, bias voltage and current. YBCO and VO_2 are that kind of materials and their conductivity controlled by switching the temperature. Using YBCO metamaterials in sensing devices for the purpose of detection is one of attractive application of this film. Moreover, since conductivity of VO_2 depends on temperature, the phase of VO_2 can easily change from insulator to metal. Thus, spectroscopy devices, tunable filters and bolometers are potential applications of this film.

In conclusion, metamaterials or 2 dimensional types of them called metasurfaces took attention in terahertz region in recent years. Metamaterials are different materials since their material properties such as ε and μ can be changed to demanding requirements. Therefore, using metamaterials or metasurfaces in terahertz time domain spectroscopy system with different films such as superconductors and metal insulator transition materials at different temperatures is very advantageous to analyze their conductive properties. Therefore, using THz-TDS system is a useful method to study ε as a function of temperature.

REFERENCES

[1] Y. S. Lee. Principles of terahertz science and technology. *Springer Science+Business Media LLC, 2009.*

[2] B. Ferguson, Xi-Cheng Zhang. Materials for terahertz science and technology. *Nature Materials.* 1, 26-33 (2002). DOI:10.1038/nmat708

[3] J. M. Jornet, I. F. Akyildiz. *Channel modelling and capacity analysis for electromagnetic wireless nanonetworks in the terahertz band*. IEEE Transcations on Wireless Communications, Vol. 10, No.10, October 2011

[4] X. C. Zhang and J. Xu. Introduction to THz wave photonics. *Springer Science+Business Media, LLC,* 2010

[5] W. Withayachumnankul, D. Abbott. Metamaterials in thz regime. *IEEE Photonics Journal.* Vol 1, No 2, August 2009.

[6] M. Wegener, J. Zhou, T. Koschny, S. Linden, C. Enrika and C. M. Soukoulis. Magnetic responce of metamaterials at 100 terahertz. *Science*. Vol. 306, Issue 57000, pp. 1351-1353. DOI: 10.1126/science.1105371

[7] R. Liu, T. J. Cui, D. Huang, B. Zhao, D. R. Smith. Description and explanation of electromagnetic behaviors in artificial metamaterials based on effective medium theory. *Phys. Rev*. E 76, 026606. 2007.

[8] C. L. Holloway, E. F. Kuester, J. A. Gordon, J. O'Hara, J. Booth and D. R. Smith. An overview of the theory and applications of metasurfaces: the two dimesional equivalents of metamaterials. *IEEE Antennas and Propagation Magazine*, 54(2):10-35, April 2012.

[9]W. Withayachumnankul, M. Naftaly. Fundametals of measurement in terahertz time-domain spectroscopy. *J Infrared Milli Terahz Waves, Springer*, 2013 DOI 10.1007/S10762-013-0042-z

[10] R. A. Cheville. Perspective on thz time domain spectroscopy. *Journal of Optical Society of Korea*, Vol 8, No. 1, March 2004 pp. 34-52

[11] J. R. Schrieffer, J. S. Brooks. Handbook of high-temperature superconductivity: theory and experiment. *Springer*. ISBN: 978-0-387-35071-4 (Print) 978-0-387-68734-6 (Online).

[12] J. M. O. Zide, A. C. Gossard, A. J. Taylor, H. T. Chen, W. J. Padilla and R. D. Averitt. Active terahertz metamaterial devices. *Nature Publishing Group.* Vol 444, DOI:10.1038/nature05343, Nov 2006.

[13] H. Chen, A. J. Taylor and Nanfang Yu. A review of metasurfaces: physics and applications. *Rep. Prog. Phys*. 79, 2016.

[14] Q. Yang, J. Gu, D. Wang, X. Zhang, Z. Tian, C. Ouyang, R. Singh, J. Han and W. Zhang. *Optics Express*. Vol. 22, No 21, DOI: 10.1364/OE.22.025931, Oct 2014.

[15] S. J. Park, J. T. Hong, S. J. Choi. H. S. Kim, W. K. Park, S. T. Han, J. Y. Park, S. Lee, D. S. Kim and Y. H. Ahn. Detection of microorganisms using terahertz metamaterials. *Scientific Reports.* 4:4988. DOI: 10.1038/srep04988

[16] D. Shrekenhamer, J. Montoya, S. Krishna, W. J. Padilla. Four-color metamaterial absorber thz spatial ligth modulator. *Adv. Optical Mater*. DOI: 10.1002/ADOM.201300265, 2013.

[17] S. L. Dexheimer. Terahertz spectroscopy principles and applications. *CRC Press*, 2007.

[18] H. J. Bakker, G. C. Cho, H. Kurz, Q. Wu and X. C. Zhang. Distoriton of terahertz pulses in electro-optic sampling. *J. Opt. Soc. Am*. B/Vol. 15, No.6 June 1998

[19] A. U. Sokolnikov. THz identification for defense and security purposes. *World Scientific Publishing* Co. Pte. Ltd, 2013

[20] B. E. A. Saleh, M. C. Teich. Fundamentals of Photonics. *Wiley Series in Pure and Applied Optics*, 2013

[21] W. Zouaghi, M. D. Thomson, K. Rabia, R. Hahn, V. Blank and H. G. Roskos. Broadband terahertz spectroscopy: principles, fundamental research and potential for industrial applications. *Eur. J. Phys.* 34 (2013) S179-S199. Oct 2013.

[22] F. Sanjuan and J. O. Tocho. Optical properties of silicon, sapphire, silica and glass in the terahertz range. *Latin American Optics and Photonics Technical Digest OSA* 2012.

[23] J. Maxwell. A dynamical theory of the electromagnetic field. *Philos. Trans. R. Soc. Lond*. 155,459-512 (1865).

[24] E. Hecht. Optics, 4th ed. *Pearson, NJ*. 2003

[25] G. Fowles, Introduction to modern optics, 1st ed. *Dover Publications, New York*.1990.

[26] M.Born, E. Wolf. Principles of optics, 7th edn. *Cambridge University Press, Cambridge. 1999*

[27] M. C. Nuss and J. Orenstein. Millimeter and submillimeter wave spectroscopy of solids. *Springer-Verlag Berlin Heidelberg*, 1998.

[28] G. Jnawali, Y. Rao, H. Yan and T. F. Heinz. Observation of a transient decrease in terahertz conductivity of single-layer graphene induced by ultrafast optical excitation. *Nano Lett*. 2013, 13, 524-530

[29] M. Walther, D. G. Cooke, C. Sherstan, M. Hajar, M. R. Freeman and F. A. Hegmann. Terahertz conductivity of thin films at the metal-insulator percolation transition. *Physical Review* B 76, 125408 (2007).

[30] P. Mandal, A. Speck, C. Ko and S. Ramanathan. Terahertz spectroscopy studies on epitaxial vanadium dioxide thin films across the metal-insulator transition. *Optics Letters*. Vol 36, No. 10. (2011).

[31] A. K. Azad, H. Yang, S. A. Trugman, Q. X. Jia, J. Taylor, R. Singh, J. Xiong and H. T. Chen. Tuning the resonance in high temperaturesuperconducting terahertz metamaterials. *Phys. Rev. Lett*., 105:247402, 2010.

[32] S. Cibell, R. Leoni, P. Carelli, F. Valmorra, M. Beck, G. Scalari, C. Maissen and J. Faist. Superconducting complementary metasurfaces for thz ultrasong light-matter coupling. *New Journal of Physics.* 16 (2014) 033005

[33] A. Durrant. Quantum physics of matter. *The Open University*. ISBN 0 7503 0721 8. 2000.

[34] G. Lanzani. Photophysics of molecular materials from single molecules to single crystals.*WILEY-VCH Verlag GmbH & Co, KGaA.* ISBN-13: 978-3-527-40456-8

[35] J. D. Patterson and B. C. Bailey. Solid-state physics introduction to theory. *Springer Publishing Companny.* ISBN-10 3-540-24115-9. 2007

[36] A. C. Rose-Innes and E. H. Rhoderick. Introduction to superconductivity. Revised 2nd edn. Pergamon Press. 1978

[37] M. Tinkham . Introduction to superconductivity. 2nd edn. *Dover Publication, Inc*. June 2004.

[38] Y. Demirhan, H. Alaboz, M. A. Nebioglu, B. Mulla, M. Akkaya, H. Altan, C. Sabah and L. Ozyuzer. Fourcross shaped metamaterial filters fabricated from high temperature superconducting YBCO and Au thin films for terahertz waves. *Superconductors Science and Technology*, 2017

[39] S. D. Brorson, R. Buhleier, I. E. Trofimov, J. O. White, Ch. Ludwig, F. F. Balakirev, H.-U. Habermeier and J. Kuhl. Electrodynamics of high temperature superconductors investigated with coherent terahertz pulse spectroscopy. *J. Opt. Soc. Am*. B, 13(9):1979-1993, Sep, 1996.

[40] O. G. Vendik, I. B. Vendik and D. I. Kaparkov. Emperical model of the microwave properties of high temperature superconductors. *IEEE Transcations on Microwave Theory and Techniques*, 46(5):469-478, May 1998.

[41] N. F. Mott. Metal-insulator transition. *Reviews of Modern Physics*. Vol 40, No 4, Oct 1968.

[42] Q-Y. Wen, H-W Zhang, Q-H. Yang, Y-S. Xie, K. Chen and Y-L Liu. Terahertz metamaterials with VO_2 cut-wires for thermal tunability.*Appl. Phys. Lett*. 97, 021111 (2010); doi: 10.1063/1.3463466.

[43] Y. Zhou, X. Chen, C. Ko, Z. Yang, C. Mouli and S. Ramanathan. *IEEE Electron Device Lett*. 2013, 34, 202-208.

[44] M. A. Katts, R. Blanchard, S. Zhang, P. Genevet, C. Ko, S. Ramanathan and F. Capasso. *F. Phys. Rev* X 2013, 3, 041004-041010.

[45] P. U. Jepsen, B. M. Fischer, A. Thoman, H. Helm, J. Y. Suh, R. Lopez and R. F. Haglund. Metal insulator phase transition in a VO_2 thin film observed with terahertz spectroscopy. *Phys. Rev.* B 74, 205103 (2006). DOI: 10.1103/PhysRevB.74.205103

[46] L. Wei, C. Sheng-jiang, W. Xiang-hui, L. Lie and B. Jın-jun. A thermally tunable terahertz bandpass filter with insulator-metal phase transition of VO_2 thin film. *Optoelectronics Letters.* Vol. 10 No.3, May 2014. DOI: 10.1007/s11801-014-3236-2

[47] M. Walther, D. G. Cooke, C. Sherstan, M. Hajar, M. R. Freeman and F. A. Hegmann. Terahertz conductivity of thin gold films at the metal-insulator percolation transition. *Phys. Rev*. B 76, 125408 (2007). DOI: 10.1103/PhysRevB.76.125408.

[48] C. Winnewisser, F. Lewen, J. Weinzierl and H. Helm. Transmission features of frequency-selective components in the far infrared determined by terahertz time domain spectroscopy. *Appl. Opt.*, 38 (18), 3961 (1999).